Design & Fabrication of a High Temperature AC - Susceptometer

A Thesis

submitted to
Indian Institute of Science Education and Research Pune
in partial fulfillment of the requirements for the
BS-MS Dual Degree Programme

by

Shantanu

IISER PUNE

Indian Institute of Science Education and Research Pune
Dr. Homi Bhabha Road,
Pashan, Pune 411008, INDIA

May, 2025

Supervisor: Dr. Ashna Bajpai

Certificate

This is to certify that this dissertation entitled *Design & Fabrication of a High Temperature AC - Susceptometer* towards the partial fulfilment of the BS-MS dual degree programme at the Indian Institute of Science Education and Research, Pune represents study/work carried out by Shantanu at Indian Institute of Science Education and Research under the supervision of Dr. Ashna Bajpai, Associate Professor, Department of Physics , during the academic year January 2024 to December 2024, later extended till May 2025.

Dr. Ashna Bajpai

Committee:

Dr. Ashna Bajpai

Dr. Sunil Nair

This thesis is dedicated to
my family and all my friends,
wherever they are...

Declaration

I hereby declare that the matter embodied in the report entitled *Design & Fabrication of a High Temperature AC - Susceptometer*, are the results of the work carried out by me at the Department of Physics, Indian Institute of Science Education and Research, Pune, under the supervision of Dr. Ashna Bajpai and the same has not been submitted elsewhere for any other degree.

Shantanu

Acknowledgements

First and foremost, I would like to thank my supervisor, Dr. Ashna Bajpai, for her expert guidance throughout the course of this project, without which none of this would have been possible. Her constant support and faith in me, especially during the tough times I have had, be it professionally regarding this project or personally regarding my career, mental and physical health, is the reason I have been able to do this.

Then, I would like to thank my project expert Dr. Sunil Nair, for his expert advice and providing access to his lab facilities. Then, I would like to thank all the lab members I have had throughout the year for help regarding this project, from my lab Dr. Durgesh, Ajad, Amit, Homesh, Ananth, Tanmayee, Shashwat, Naveen, Abhiram, Aparna, Hemabindu and Harshdeep, Rohit and Dr. Vikram from Sunil sir's lab. Also, I would like to thank Nilesh sir and Kathikeyan for helping me in this project.

I would like to thank my roommate and my friend, Monbikash and my friend Subhajit. I would also like to thank the game Valorant, for getting me through my college life, and all the friends that I have made through it, like Neil etc., and all of my teammates I have had for various tournaments, for all the fun times I have had and for some of the best memories of my college life. From my batch, I would like to thank Chirayu and Sarvesh. And a special thanks to all my juniors Shreedhar, Mihir, Abhisekh, Parth, Harshwardhan and Hritik for making my final year fun.

Also, I would like to thank my counsellor Parnika, for keeping a check on me and helping me out in tough times.

Last but not least, I would like to thank my father, Rajesh Kumar, my mother, Suman, and my sister, Ritika, for always believing in me and my abilities, and for their constant support. And a final thanks to all of my close friends, Ishant, Ruchi, Shreya, Kalyani, Ankita, Raunak, Shiven etc. for being there for me through all these years, I can't thank them enough.

And in the end, a final thanks to myself too, thank you Shantanu!

Abstract

This thesis presents the design and fabrication of a high-temperature AC susceptometer aimed at measuring the linear and non linear ac-susceptibility (χ) of magnetic materials with their transition temperature above the room temperature. The work involves both linear and non-linear harmonic analysis, with a primary focus on understanding the behaviour of first and higher harmonics in the material as it transitions through its Curie point. The initial stages of the project involved preliminary experiments conducted on using an existing ac-χ set up which was designed and fabricated for the measurement of linear and non linear susceptibility at cryogenic temperatures, down to 77 K. Using this set up, linear and non linear ac-χ measurements were recorded for two ferromagnetic samples, Ni and CrO_2. Ni was measurened in two morphology, Ni Foam and Ni Plate. Notabaly, CrO_2 is a half metallic ferromagnet with $T_C \sim 393$ K and Ni is well known elemental ferromagnets with $T_c \sim 627$ K.

A significant portion of the work was dedicated to the design and fabrication of the high-temperature setup. This project required multiple iterations to design a heater capable of achieving the necessary high temperatures. Both Nichrome and Kanthal wires were tested for high temperature heater, wound in non inductive geometry. A dimmerstat was used to regulate the power input, and Lakeshore temperature controller for measuring temperature. After several trials, the final heater used was a Nichrome wire wound inductively on a ceramic rod. This heater reached a temperature of around 750 K under vacuum condition, exceeding the requirements for the Nickel sample.

Once the heater was optimized, the final step was the integration of all components into a cohesive high-temperature susceptometer system. This included the fabrication of key parts such as the secondary coil, sample rod, and the inner and outer Dewar systems, which were assembled from metal, hylum plates, rods, and teflon. After assembling all the components and setting up the system, a final set of measurements was conducted on a Nickel foam. A fast temperature scan, in which data is recorded while heating the sample from below its T_C (without controlling the temperature) was conducted so as to measure the temperature variation of both first and the third harmonic of ac susceptibility of Nickel. This showed clear paramagnetic to ferromagnetic transition, in both first and third harmonics in the vicinity of T_C. However, the measurement could not be extended to take reasonable number of data points in the paramagnetic region, but still confirming the functionality of the setup. While sample holder needs to be modified for controlled measurements, this work lays the groundwork for future studies in high-temperature magnetism, opening avenues for exploring new materials and refining measurement techniques at elevated temperatures.

Contents

List of Figures

List of Tables

Chapter 1

Introduction

The key aim of this project is to design and fabricate a high temperature ac-susceptometer that would enable us to identify and characterize magnetic phase transitions, especially for samples with magnetic transition above room temperature. This chapter contains a brief overview on magnetic materials and the technique of ac-susceptibility along with special emphasis to ferromagnetic Ni and CrO_2.

1.1 Magnetic properties

We can say that the magnetic property of a material arises because of the magnetic moments and electronic spins in them. The magnetic moment can arise from two main sources[23] -

- Electron spin - Magnetic moment can be generated because of an electron's intrinsic angular momentum
- Orbital motion - Another way it can be generated is when the electron revolves around the nucleus giving rise to a circulating charge

1.2 Magnetization

Magnetization, or $\boldsymbol{M}$ is a fundamental property of material. In brief, it describes the response of a material to an external magnetic field. It is defined as the net magnetic moment density, or magnetic moment per unit volume of a magnetic sample, where every atom that constitutes that magnetic sample has a magnetic moment of their own. This vector field $\boldsymbol{M}$ is considered to be smooth and continuous everywhere except for the edges of the magnetic material [4].

Now, on introducing a magnetic field $\boldsymbol{H}$, the material gets induced magnetization, $\boldsymbol{B}$. In a magnetic solid, their relation can be expressed by the equation -

$$\boldsymbol{B} = \mu_0(\boldsymbol{H} + \boldsymbol{M}) \tag{1.1}$$

where μ_0 is th magnetic permeability of free space.

Now in special case, like in materials such as paramagnets or ferromagnets,

$$\boldsymbol{M} = \chi \boldsymbol{H} \tag{1.2}$$

This χ is called magnetic susceptibility. It is a dimensionless quantity which is defined as the ratio of a material's magnetization to the applied magnetic field strength. It can be expressed in the form of a equation as follows -

$$\chi = \lim_{\boldsymbol{H} \to 0} \frac{\boldsymbol{M}}{\boldsymbol{H}} \tag{1.3}$$

Sometimes, it is also expressed as differential susceptibility in the following form -

$$\chi = \frac{\partial \boldsymbol{M}}{\partial \boldsymbol{H}} \tag{1.4}$$

1.3 Magnetic Materials and Behaviour

All materials showcase different magnetic behaviour, depending on how they respond to an external magnetic field and their internal electronic configuration. Main reason behind this kind of behaviour is of the electronic spins and how they interact within a material. These types of behaviour can be broadly described in five categories as listed below -

1.3.1 Diamagnetism

When an external magnetic field is applied, a diamagnetic material will showcase a weak repulsion. It happens because the induced magnetic moment on applying the field is in the direction opposite to it. These materials also showcase no magnetic dipole moment because all of its electrons are paired.

Some good examples of diamagnetic material will include copper, gold, bismuth and graphite[2]. Their magnetic susceptibility is always negative, generally in the range of -10^{-6} to -10^{-5}.

1.3.2 Paramagnetism

Paramagnetism arises from the presence of unpaired electrons in atoms or ions, which possess intrinsic magnetic moments due to their spin and orbital angular momentum. In the absence of an external magnetic field, these moments are randomly oriented, resulting in no net magnetization. However, when an external field is applied, the magnetic moments tend to align with the field, leading to a net positive magnetization. The effect is generally weak and follows Curie's Law at high temperatures, indicating an inverse relationship between susceptibility and temperature [16].

The Curie-Weiss law -

$$\chi = \frac{C}{T - \theta} \tag{1.5}$$

where χ is the magnetic susceptibility, C is the Curie constant, T is the absolute temperature (in Kelvin), and θ is the Weiss constant (also known as the Curie-Weiss temperature). This equation describes the temperature dependence of the magnetic susceptibility in paramagnetic materials above the Curie temperature. [16]

For paramagnetic materials, when $\theta = 0$, the Curie-Weiss equation reduces to the standard Curie Law:

$$\chi = \frac{C}{T} \tag{1.6}$$

Some good examples would include aluminium.[16] On the removal of external magnetic field, these materials would not retain any magnetization.

1.3.3 Ferromagnetism

When an external magnetic field is applied, a ferromagnetic material will showcase a strong attraction. This happens because magnetic moments gets aligned in a specific region known as domain. Inside the domain, the magnetic moments of atoms are spontaneously aligned in the same direction due to exchange interaction. These domains form naturally even without an external magnetic field, as a way to minimize the material's total magnetic energy, particularly the magnetostatic energy[6]. These domains are the regions in a ferromagnetic material where magnetic moments are aligned uniformly. The boundaries of these domains are called domain walls, and the movement and interaction of these walls helps us understand some macroscopic magnetic properties of a material.

Now in a domain, this alignment happens within a domain because of the strong exchange interactions among neighbouring atoms, which causes their spins to align in the same direction. Even after the removal of external magnetic field, a ferromagnetic material can retain their magnetization.

These material showcases positive magnetic susceptibility. For ferromagnetic materials, $\theta > 0$ in the Curie- Weiss law, indicating a transition temperature T_C where spontaneous magnetization appears.

The exchange interaction Hamiltonian for ferromagnets can be described as:

$$H = -\sum_{i,j} J_{ij} \mathbf{S}_i \cdot \mathbf{S}_j \tag{1.7}$$

In this expression, H denotes the total magnetic interaction energy of the system. The sum runs over all pairs of spins located at lattice sites i and j. The quantity J_{ij} is the exchange interaction constant, which determines the nature of the spin interaction: a positive J_{ij} favours parallel spin alignment (ferromagnetic interaction), while a negative J_{ij} favours antiparallel alignment (antiferromagnetic interaction). The vectors $\mathbf{S}_i$ and $\mathbf{S}_j$ represent the spin at sites i and j, respectively, and $\mathbf{S}_i \cdot \mathbf{S}_j$ is their dot product, indicating the degree of alignment between the spins. In ferromagnetic materials, the exchange integral J_{ij} is strictly positive, ensuring that the spins align in the same direction, leading to spontaneous magnetization.

The ferromagnetic behaviour can be understood using the Weiss molecular field model, which proposes that for aligning the individual magnetic moments, there should be a presence of an internal mean field. This model serves as a theoretical foundation for explaining how spins in ferromagnetic materials collectively align and how they interact with external magnetic fields.

Some good examples of ferromagnetic material would be nickel, cobalt and iron. In further section of this chapter, we will dive more into the magnetic properties of Nickel since it would be our primary element of focus for this project.

1.3.4 Antiferromagnetism

In antiferromagnetic materials, the magnetic moments of the adjacent atoms gets aligned in the opposite direction. This leads to no net magnetization at macroscopic level. This type of thing happens because of the unique crystal structure of the material that ultimately promotes the alternating spin alignment. These ordering of spins are temperature dependent and at above a certain temperature, called the Néel temperature (T_N), antiferromagnetic materials become paramagnetic. Also, for antiferromagnetic materials, $\theta < 0$, implying a tendency for anti-aligned spin arrangements.

Some good examples include manganese oxide and chromium.

1.3.5 Ferrimagnetism

Ferrimagnets are like antiferromagnets, that is they both have the opposing magnetic moments, but the difference being that these opposite moments are unequal, which in turn results in some net magnetization. This happens because of the crystal structure of the material that contains some magnetic sublattices with them having different magnitude of magnetic moments.

Some good examples include magnetite and ferrites.

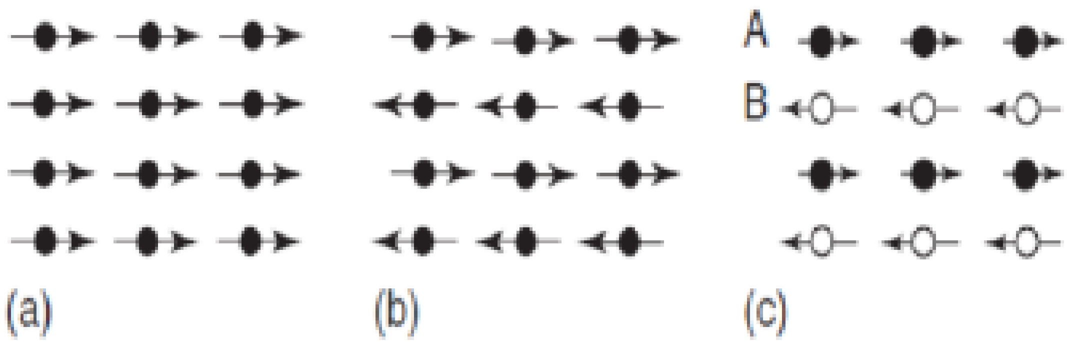

Figure 1.1: Schematic spin orientations in various types of magnetic ordering structures: (a) Ferromagnetism, (b) Antiferromagnetism, (c) Ferrimagnetism [9]

1.4 AC- Magnetic Susceptibility (AC-χ)

AC magnetic susceptibility is a powerful tool that can be used for the investigation of the dynamic magnetic properties of the given material. In this section we will explore its theoretical background, measurement techniques, and some applications in condensed matter physics.

1.4.1 Introduction

To analyse a material's magnetic behaviour, a sinusoidal magnetic field is applied:

$$H = H_{dc} + H_{ac}\cos(\omega t), \tag{1.8}$$

where $\omega = 2\pi f$ represents the field frequency. The material's response to this varying field is known as AC magnetic susceptibility. Assuming a linear response, susceptibility is given by:

$$\chi_{ac} = \frac{M_{ac}}{H_{ac}}. \tag{1.9}$$

However, most materials, it exhibits a non-linear response to an external field, requiring an expanded expression for magnetization[3]:

$$M = M_0 + \chi_1 H + \chi_2 H^2 + \chi_3 H^3 + \dots, \tag{1.10}$$

where χ_1 denotes linear susceptibility and M_0 represents spontaneous magnetization due to internal fields. Typically, only odd-order terms contribute, unless an internal symmetry-breaking field is present, allowing even-order terms.

So when subjected to an oscillating magnetic field $H(t) = H_0 e^{i\omega t}$, we get the resulting magnetization as:

$$M(t) = \chi' H_0 e^{i\omega t} + i\chi'' H_0 e^{i\omega t} \tag{1.11}$$

where, $\chi'(\omega)$ is the real part (in-phase response), representing reversible magnetization and $\chi''(\omega)$ is the imaginary part (out-of-phase response).

1.4.2 Complex Susceptibility

From what we saw above, we can say that AC susceptibility is inherently complex and can be expressed as:

$$\chi_{ac} = \chi_r + i\chi_i, \tag{1.12}$$

where:

- χ_r is the in-phase component aligned with the applied AC field.
- χ_i is the out-of-phase component, indicating dissipative effects.

Since magnetization is also time-dependent, it can be expressed as:

$$M = M_0 + m\cos(\omega t - \theta). \tag{1.13}$$

From this, the real and imaginary components of susceptibility can be written as:

$$\chi_r = \frac{m\cos\theta}{H_{ac}}, \quad \chi_i = \frac{m\sin\theta}{H_{ac}}. \tag{1.14}$$

Extending this to higher-order susceptibilities, magnetization takes the form:

$$M = M_0 + H_{ac}\sum_{n=1}^{\infty}(\chi_r^n \cos(n\omega t) + \chi_i^n \sin(n\omega t)). \tag{1.15}$$

From this, susceptibility of order n can be observed at frequency $n\omega$ (e.g., third-order susceptibility χ_3 appears at 3ω). This reveals that higher-order susceptibilities correspond to higher harmonics.

1.4.3 Measurement of AC Susceptibility

AC susceptibility is typically measured using a lock-in amplifier and an oscillating magnetic field. Key parameters include:

- Frequency dependence (ω): useful for studying relaxation phenomena.
- Temperature dependence (T): helps identify phase transitions.
- Field amplitude (H): reveals magnetization dynamics in presence of external magnetic field

1.4.4 AC Susceptibility and Phase Transitions

Near phase transitions, susceptibility follows a power law [28]:

$$\chi' \propto |T - T_c|^{-\gamma} \tag{1.16}$$

where γ is a critical exponent.

Further analysis of the susceptibility data near the Curie temperature allows estimation of critical exponents. The divergence of the linear susceptibility χ_1 yields the exponent γ, while the behaviour of χ_3 reflects non-linear scaling near T_C. These exponents help classify the transition and can be compared with predictions from universality classes like the 3D Heisenberg model.

1.4.5 Experimental Techniques

There are different experimental techniques that can be used for studying this. For example, magnetic susceptibility using a DC magnetic field can be measured with high sensitivity using a Superconducting Quantum Interference Device (SQUID) magnetometer or a Vibrating Sample Magnetometer (VSM). SQUID magnetometers detect extremely small magnetic signals by measuring changes in magnetic flux through superconducting loops, making them ideal for studying weakly magnetic or low-temperature samples. VSM, on the other hand, measures the magnetic moment induced in a sample by detecting the voltage generated in pickup coils as the sample vibrates in a uniform magnetic field. Both techniques allow precise characterization of the field-dependent magnetization $M(H)$, from which the dc susceptibility is derived.

Additionally, the Inductive Coil Method relies on electromagnetic induction to detect the AC magnetic response of a material, providing valuable insights into its dynamic magnetic behaviour. We will be using this particular technique in our project for studying properties associated with ac-χ in our project for Nickel and other samples.

1.4.6 Frequency Dependence and Regimes

The system's response time τ determines the susceptibility regime:

- When $\omega \gg 1/\tau$, **adiabatic susceptibility** is measured.

- When $\omega \ll 1/\tau$, **isothermal susceptibility** is obtained.

- When $\omega \approx 1/\tau$, the system is in the intermediate regime

1.4.7 Standard Trend of Linear and Non Linear Susceptibility Responses Across Temperature for Some Magnetic Materials

- A paramagnetic material will simply showcase an inverse relation with the temperature as predicted by the Curie-Weiss law.

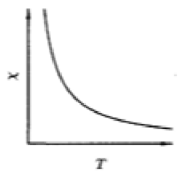

Figure 1.2: χ v T for paramagnets[4]

- Here in figure 1.3, we can clearly see that in ferromagnets, the first order susceptibility χ_1 diverges at T_C, and is positive. After T_C, the material undergoes a paramagnetic transition. Meanwhile χ_2 is negative and diverges at T_C. χ_3 is negative before T_C and showcases a sharp discontinuity at T_C, and later becomes negative.

- In antiferromagnetic materials, the linear susceptibility (χ_1) reaches its maximum at the Néel temperature (T_N). Below this transition, as the temperature decreases, χ_1 gradually approaches zero. Above T_N, the material undergoes a transition from the antiferromagnetic to the paramagnetic phase. Meanwhile (χ_2) remains zero due to the absence of a spontaneous symmetry-breaking field. And (χ_3) is positive below T_N but rapidly diminishes as the temperature decreases further. In the paramagnetic regime near T_N, the sign of χ_3 can be either positive or negative, depending on the coordination number However, as the temperature increases, χ_3 gradually approaches zero[10].

1.4.8 Physical Interpretation

From taking reference from the above section and so on, these can be taken as the physical interpretation of these ac magnetic susceptibilities trend -

- Ferromagnetic and Paramagnetic Materials : Ferromagnets exhibit a large χ' below the Curie temperature (T_C) and χ'' increases near T_C, indicating domain wall motion.
- Antiferromagnetic Materials : A peak in χ' occurs at the Néel temperature (T_N), signifying a transition to an ordered state and the energy dissipation is typically small.
- Spin Glasses and Superconductors : Spin glasses are disordered magnetic systems characterized by competing interactions and frustration, leading to a frozen magnetic state at low temperatures [19]. Superconductors are materials that exhibit

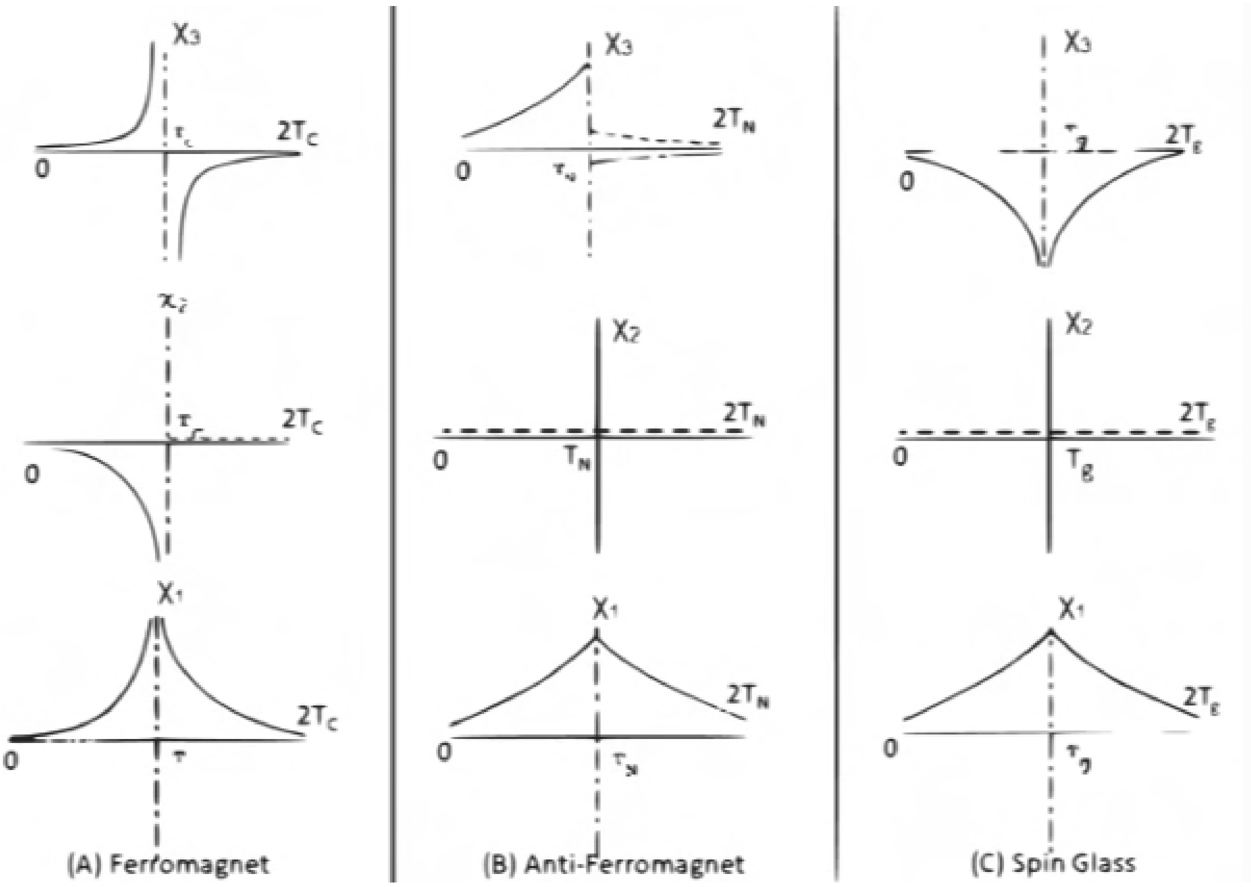

Figure 1.3: Schematic of linear and nonlinear magnetic susceptibilities in (A) FM, (B) AFM and (C) SG[10]

zero electrical resistance and expel magnetic fields below a critical temperature [25]. Spin glasses show frequency-dependent peaks in χ' while superconductors exhibit a sharp drop in χ' below T_c due to the Meissner effect.

1.4.9 Applications of AC Susceptibility

AC magnetic susceptibility is a powerful method for exploring many magnetic phenomena. It is extensively used to study magnetic phase transitions, for example measuring the Curie and Néel temperatures, which mark the onset of ferromagnetic and antiferromagnetic ordering, respectively. Additionally, it also helps in analyzing spin glass behavior and magnetic relaxation, that tells us more about disordered magnetic systems. In superconductors, AC susceptibility measurements can help us examine the vortex dynamics and flux pinning effects. Furthermore, this technique is widely applied in the characterization of nanoparticles, particularly in studying their superparamagnetic properties.

1.5 Low Temperature AC - χ Set Up

A low temperature AC susceptometer was developed earlier in our laboratory to measure both linear and nonlinear magnetic susceptibilities (χ_1, χ_2, χ_3) within a cryogenic temperature range of 77 to 300 K. The design is based on a Hartshorn-type mutual inductance bridge, comprising a primary excitation coil and two secondary detection coils wound in series opposition. The primary coil generates an alternating magnetic field, inducing voltages in the secondary coils. When a sample is placed in one of the secondary coils, its magnetic response alters the induced voltage, which is detected using a lock-in amplifier. To minimize offset voltages arising from coil imperfections, adjustments such as unwinding turns or adding extra turns to the coils are performed. The mechanical assembly includes a coil system mounted on a quartz vacuum insert and a sample rod equipped with a heater and a platinum resistance thermometer for precise temperature control. The entire setup is housed within a silvered, double-walled cryogenic dewar to reduce thermal losses. This configuration allows for accurate measurement of both the real and imaginary components of AC susceptibility across a range of frequencies [7][26].

1.5.1 Lock-In Amplifier (LIA) : A Brief Introduction to its Usage

In th AC- χ experiments, lock-In Amplifier is used to send our required signals to primary coil, which in turn excite the sample, and its signal is then detected via the secondary coil. In our experiments, wires of primary coil, with a 1 Ω resistance soldered with the primary coil in series, are connected to sine-out port of LIA, whereas secondary are connected to A and B port, via the use of BNC cables.

While taking readings on LIA, one has to take care of several factors associated with the LIA, like - sensitivity, manual reserve, frequency, harmonic, input voltage etc.

1.6 Nickel

Nickel (Ni) is a metal with atomic number 28. It belongs to the transition metals in the periodic table. It has many applications and properties, but in this section, we will mainly focus on its magnetic properties.

1.6.1 Ferromagnetism in Nickel

It is one of the elemental ferromagnets along with Fe and Co. This ferromagnetic property emerges because of the alignment of the electron spins in the 3d orbital. It shows strong magnetic ordering at the room temperature. It has a relatively low coercivity, roughly around 20 Oersted, which implies that it is easy to both magnetize and demagnetize.

- **Curie Temperature:** $T_c = 627$ K (354°C). Above this it loses its permanent magnetization and transitions into a paramagnet.
- **Magnetic Moment:** $\mu = 0.606\mu_B$ per atom, in the bulk form. This is again because of the unpaired electron in 3d orbital that causes strong spin interaction leading to ferromagnetic ordering.
- **Face-Centred Cubic (FCC) Lattice:** The preferred magnetization axis is along the $\langle 111 \rangle$ direction.

1.6.2 Magnetic Susceptibility and Domains

- **Magnetic Susceptibility χ :** In its ferromagnetic state, Nickel has a high magnetic susceptibility. In the presence of a magnetic field, its domains get aligned with the direction of the field that strengthens its overall magnetization.
- **Magnetic Domains :** It has small regions called magnetic domains, which contains locally aligned spins in the absence of an external field, but gets distributed randomly through out it. In the presence of the external field, it grows in size. [24]
- **Hysteresis Loop :** It shows a typical ferromagnetic hysteresis loop.[30]

1.6.3 Anisotropy and Magnetostriction

- **Magnetocrystalline Anisotropy :** Ni showcases magnetocrystalline anisotropy, which means that its magnetization prefers some specific crystallographic direction. In a face-centred cubic (FCC) lattice, the preferred magnetization axis is along the $\langle 111 \rangle$ direction.[15]
- **Magnetostriction :** Ni shows magnetostriction behaviour, which means that it changes its shape when it is magnetized.[5]

1.7 Previous Studies on AC - Magnetic Susceptibility in Nickel

One of the foundational works in the study of non-linear AC magnetic susceptibility near magnetic phase transitions is the 1995 paper by Shirane et al., titled *"Non-linear Susceptibility of Ni near the Curie Temperature"* published in the *Journal of the Physical Society of Japan*[22]. This study presents a detailed experimental investigation of both the linear (χ_1) and third-order non-linear (χ_3) magnetic susceptibilities in high-purity nickel, focusing on their behaviour in the critical region near the Curie temperature (T_c).

Shirane et al. used a low-frequency AC susceptibility technique to measure χ_1 and χ_3 across a narrow temperature range surrounding the ferromagnetic–paramagnetic phase transition in Ni. They observed that χ_1 exhibits a well-defined peak just below T_c, a signature of the enhanced magnetic response due to increased domain wall mobility - an effect often associated with the Hopkinson peak. More notably, the third-order susceptibility χ_3 displayed a characteristic negative dip before undergoing a sign change near T_c, consistent with theoretical expectations for systems undergoing a second-order magnetic phase transition. This behaviour reflects the non-linear response of the magnetization due to anharmonic contributions and critical spin fluctuations near the transition point.

A significant challenge addressed in their study was the influence of eddy currents, which become non-negligible at higher excitation frequencies in metallic samples. These eddy currents distort the measured susceptibilities, particularly χ_3, due to induced screening fields. Shirane et al. developed a method to effectively correct for these effects, enabling a more accurate extraction of the intrinsic nonlinear magnetic response of the system. This aspect of their work remains particularly relevant for experiments involving bulk metallic samples such as nickel, and serves as a guideline for interpreting AC susceptibility data in the presence of such artifacts.

From their measurements, they extracted the critical exponents associated with the divergence of susceptibilities near T_c, reporting values of $\gamma = 1.333 \pm 0.008$ for the linear susceptibility and $\gamma_3 = 4.69 \pm 0.30$ for the third harmonic. These values are in close agreement with theoretical predictions and serve as a quantitative benchmark for characterizing ferromagnetic critical behaviour.

This study by Shirane et al. provides a foundational reference for experiments involving the detection of nonlinear susceptibilities near magnetic phase transitions. It validates the use of AC susceptibility - especially higher harmonics like χ_3—as sensitive probes for the critical behaviour in ferromagnetic systems, and offers key experimental insights that have guided the design and interpretation of similar studies, including the present work.

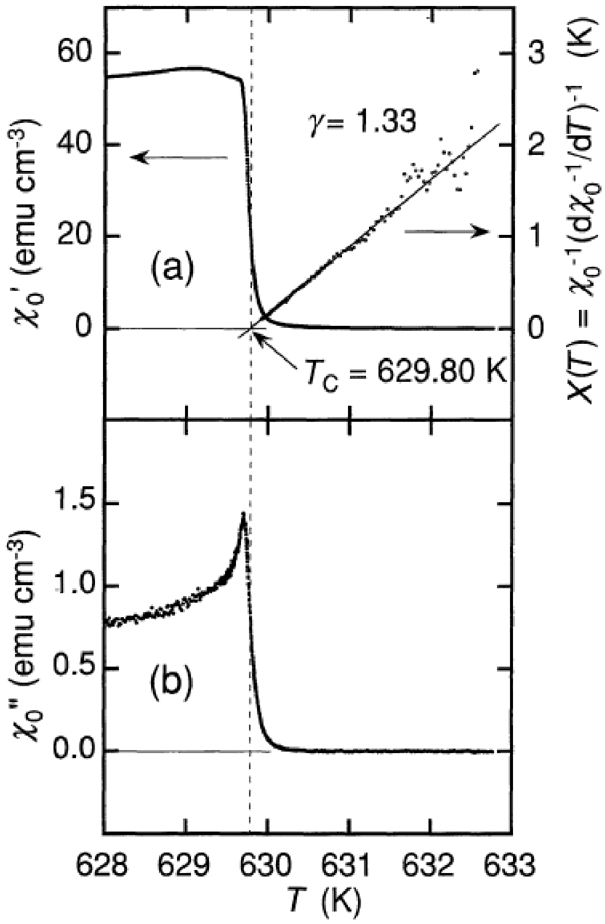

Figure 1.4: Temperature dependence of (a) the in-phase component χ_0' of the linear magnetic susceptibility and $X(T) = \chi_0'^{-1} \left(\frac{d\chi_0'^{-1}}{dT} \right)^{-1}$ (Kouvel-Fisher plot); (b) the out-of-phase component χ_0'' of the linear magnetic susceptibility, measured at $h_0 = 0.04$ Oe and at $f = 20$ Hz. The inverse of the slope of the straight line gives the value of γ and its intercept on the temperature axis gives T_C. The vertical broken line indicates T_C. [22]

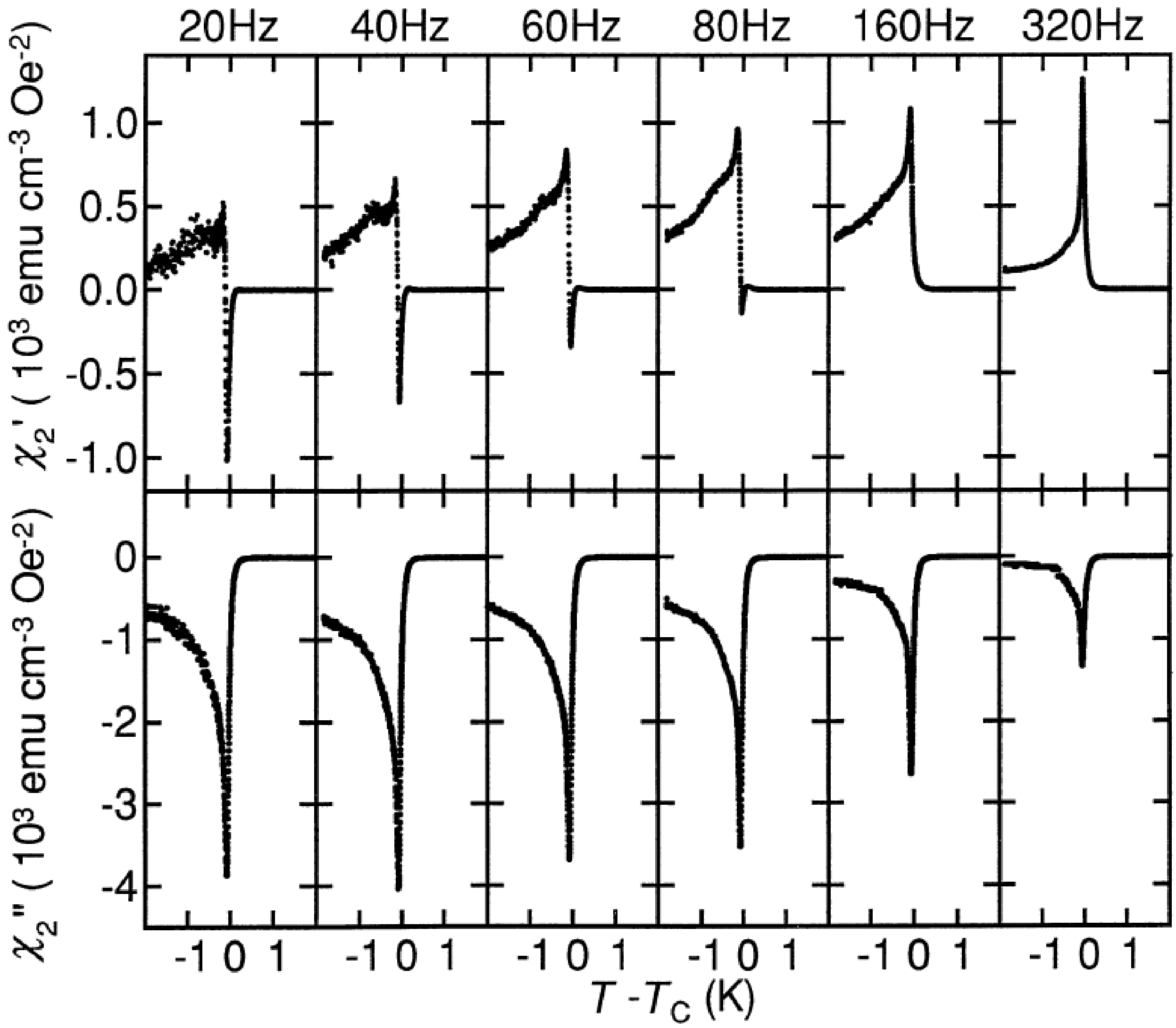

Figure 1.5: The in-phase component χ' (upper) and the out-of-phase component χ'' (lower) of the nonlinear magnetic susceptibility at various measuring frequencies, measured at the ac-field amplitude $h_0 = 0.04$ Oe.[22]

Chapter 2

Preliminary Runs on Samples with T_C Above RT

In this chapter, we will focus on the operational principles of the existing AC susceptibility setup and the Lock-In Amplifier utilized in the laboratory. It also includes a series of experimental runs comparing the sine output with the corresponding output signal of some samples like Ni. Further details are elaborated in the subsequent subsections.

2.1 Setting up Lock In Amplifier and Sample rod

In upcoming sections, if not explicitly mentioned otherwise, the value of reference frequency is 133 Hz, time constant 300 ms and the system is in A-B mode at RT. Offset was measured every time, and phase was set.

Samples with the help of GE varnish and Teflon is glued to the sapphire rod in the end of the sample rod where PRT is also attached, and then sample rod is inserted in the vertical coil from top. For measuring offset, sample rod is positioned such that sample is outside the coil. A mark was created on sample rod to identify the right length it should be hung from the top so that the sample is at the spot where the signal received is maximum.

2.2 Ni Plate v Ni Foam Runs

After understanding the basics of a Lock-In Amplifier, two Ni samples were explored, one Ni foam and other Ni plate, both of which are Sigma Aldrich samples, with 99.99 % purity, in order to run my initial runs on them, on a pre existing home made ac susceptometer in the lab. Here are some key features of the coils of this set up -

- Primary Coil :
  1. Number of turns : 1300
  2. Length : 15 cm
  3. Resistance at RT : 84.4 Ω
- Secondary Coil :
  1. Number of turns : 3000 each
  2. Length : 12 mm each
  3. Resistance at RT : 624 Ω (total)

Here, the basic aim was to measure linear and non linear ac - susceptibility in two samples of Ni, one in the form of plate and other in the form of Foam. Both are 99.9 % pure Ni samples purchased from Sigma-Aldrich. Ni is a ferromagnetic metal. The mass of the Ni foam was 4.8 mg, whereas for Ni plate was 81.9 mg.

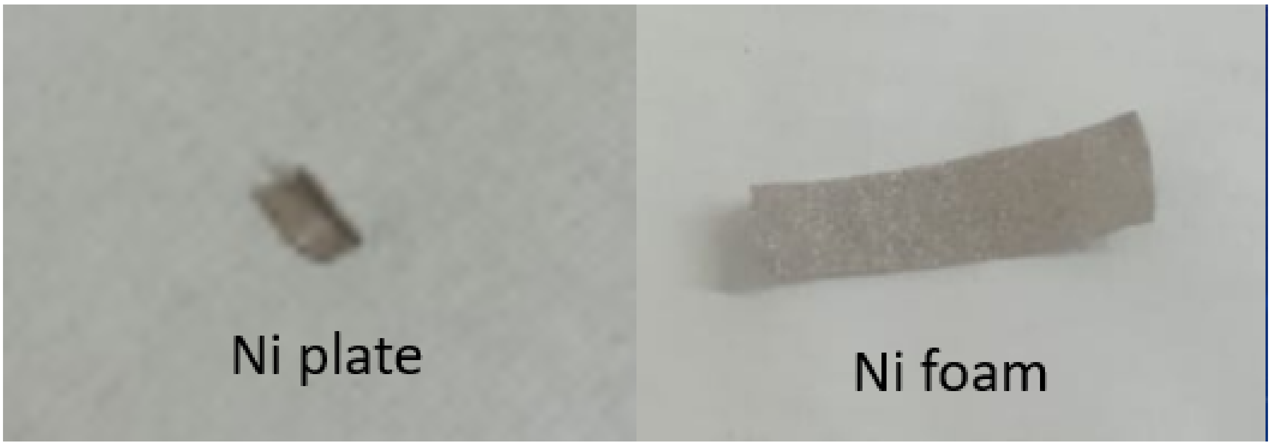

Figure 2.1: Ni plate and Ni foam

2.3 Run for Offset Variation

In this run, the variation in offset was taken versus sine-out values for first harmonic values on this ac susceptometer. For measuring offset here, sample rod is inserted in the coil without any sample attached to it and could be compared to the offset when it is measured without both rod and sample inside the coil. The values are plotted and we can see the increase in the offset with the sine-out value linearly as it was expected.

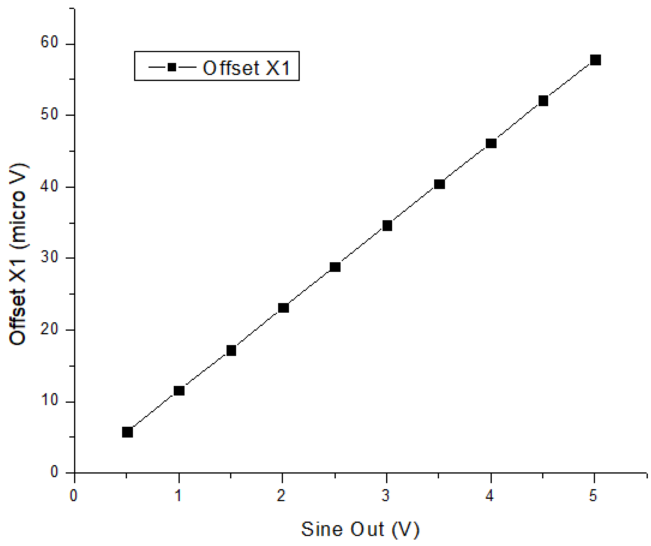

Figure 2.2: Offset : χ_i first harmonic

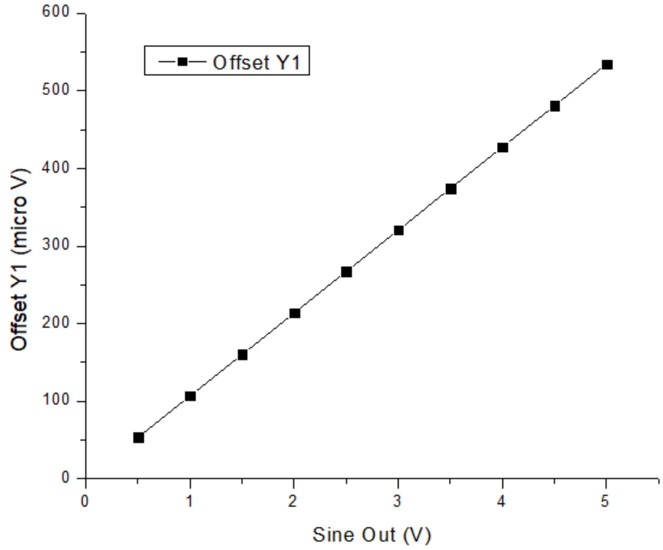

Figure 2.3: Offset : χ_r first harmonic

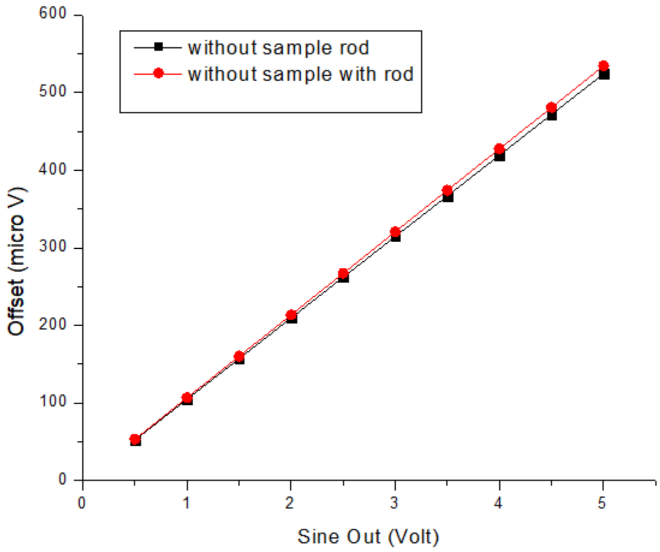

Figure 2.4: Offset : first harmonic real part

2.3.1 Ni Plate & Ni Foam : Effect of Variation in AC Magnetic Field

We will take our data as the signal measured vs the sine-out value, which corresponds to the ac-χ vs the applied magnetic field. Before starting each run, for both Ni foam and Ni plate, phase was set and offset was measured from sine-out values ranging from 0.5V to 5V with an increment of 0.5V. The results obtained are then plotted in the graphs below, which could be used for the comparison between the two. In this run, we have measured for both, the first and third harmonic, where third harmonic readings were taken twice and all are plotted together.

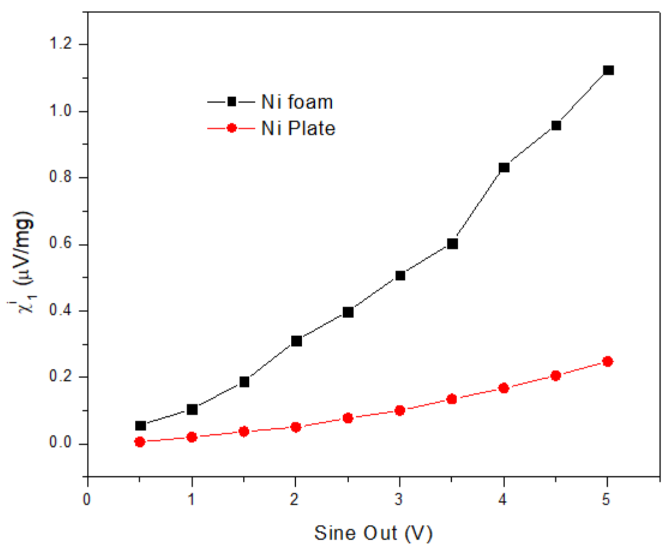

Figure 2.5: Ni plate & Ni foam, First Harmonic Imaginary Part: AC-χ vs Applied Magnetic Field (signal measured v sine-out)

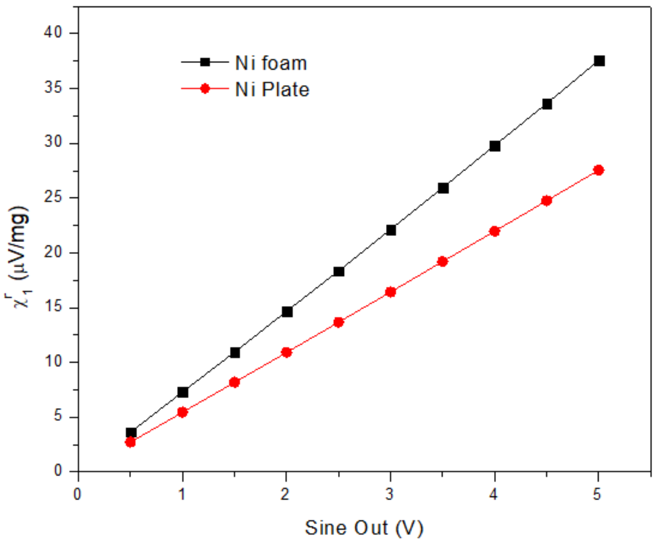

Figure 2.6: Ni plate & Ni foam, First Harmonic Real Part : AC-χ vs Applied Magnetic Field (signal measured v sine-out)

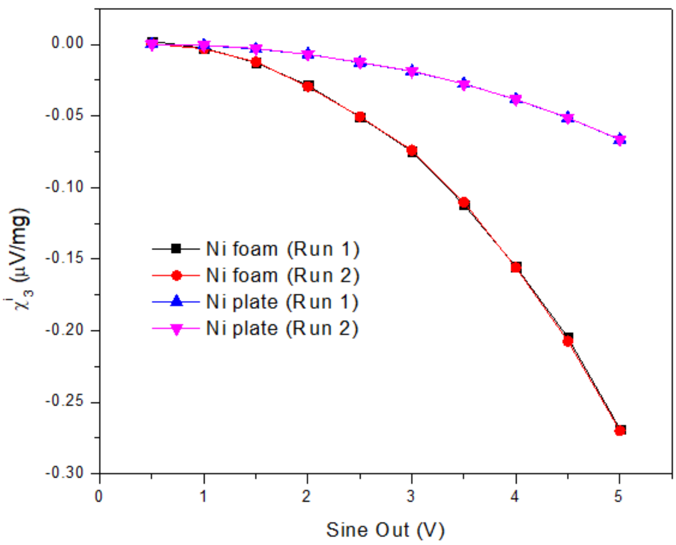

Figure 2.7: Ni plate & Ni foam, Third Harmonic Imaginary Part : AC-χ vs Applied Magnetic Field (signal measured v sine-out)

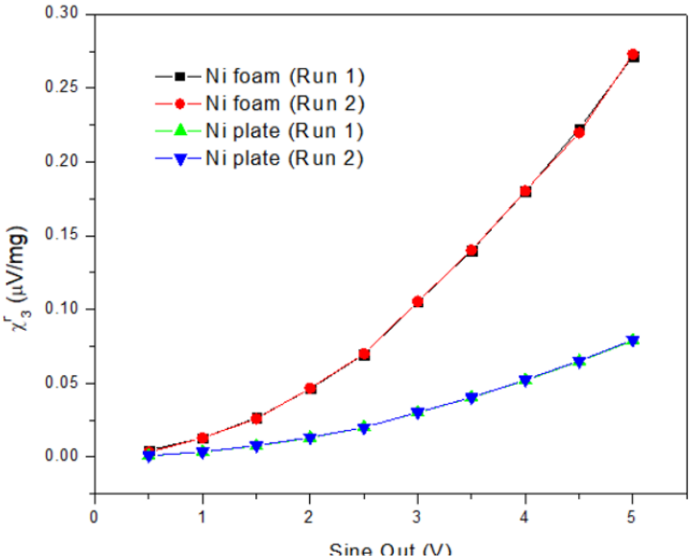

Figure 2.8: Ni plate & Ni foam, Third Harmonic Real Part : AC-χ vs Applied Magnetic Field (signal measured v sine-out)

Looking at these data in figures 2.5, 2.6,2.7 and 2.8, we observe that the signals measured for both Nickel sample were of the order of $\mu V/mg$ after normalising the values with their mass. Here we observed that the signal received from a Nickel foam is greater than a Nickel plate. Also when increasing the sine out value, this gap in the difference also widens. This difference in their signal values can be attributed to their difference in morphological structure as foam is porous and thus has a larger surface area that results into giving more signal. Also screening effect in plate is may be responsible for this. For these reasons also we ended up using Nickel foam for our runs.

Whereas the nature of the data itself, where for both imaginary and real part of the first harmonic, we can observe an almost linearly increasing data points. But for the third harmonic, it looks like an exponential function, which is decreasing for the imaginary part and increasing for the real part.

2.4 AC-χ Runs for a CrO_2 sample

Chromium dioxide (CrO_2) is a well-known half-metallic ferromagnet with nearly 100%spin polarization at the Fermi level, making it an ideal candidate for spintronic applications. It crystallizes in the rutile structure and exhibits a Curie temperature of approximately 393 K. The ferromagnetism in CrO_2 is primarily attributed to the double exchange mechanism between Cr^{4+} ions[17].

2.4.1 CrO_2 Run at Room Temperature for First, Second and Third Harmonic

Here we did an ac-χ run for CrO_2 on the same lock in amplifier, parameters as we did for Ni, the only difference being that we also measured second harmonics for CrO_2, which we didn't get for Ni. Then its plotted as shown in graphs below. We also compared the normalised value of the signals of CrO_2 with the Ni samples. The mass of the CrO_2 sample here is 106.5 mg. The graphs are as follows -

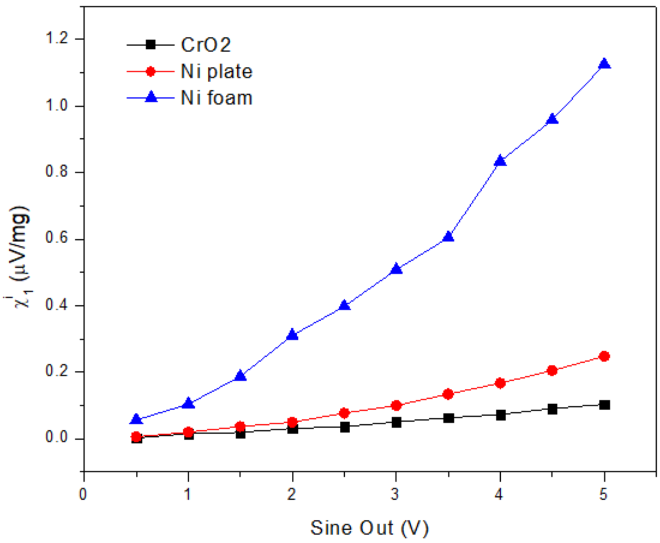

Figure 2.9: CrO_2, Ni plate & Ni foam, First Harmonic Imaginary Part : AC-χ vs Applied Magnetic Field (signal measured v sine-out)

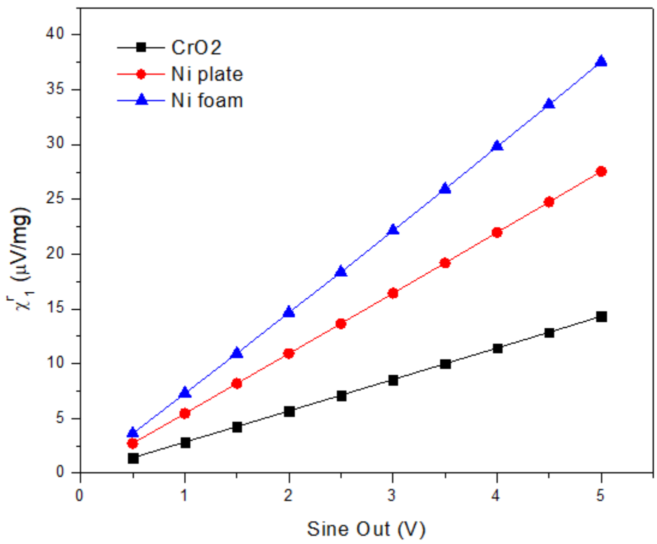

Figure 2.10: CrO_2, Ni plate & Ni foam, First Harmonic Real Part : AC-χ vs Applied Magnetic Field (signal measured v sine-out)

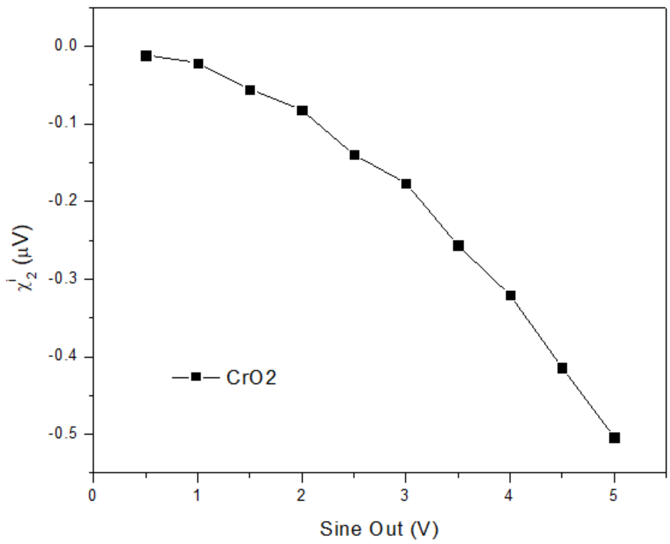

Figure 2.11: CrO_2, Second Harmonic Imaginary Part : AC-χ vs Applied Magnetic Field (signal measured v sine-out)

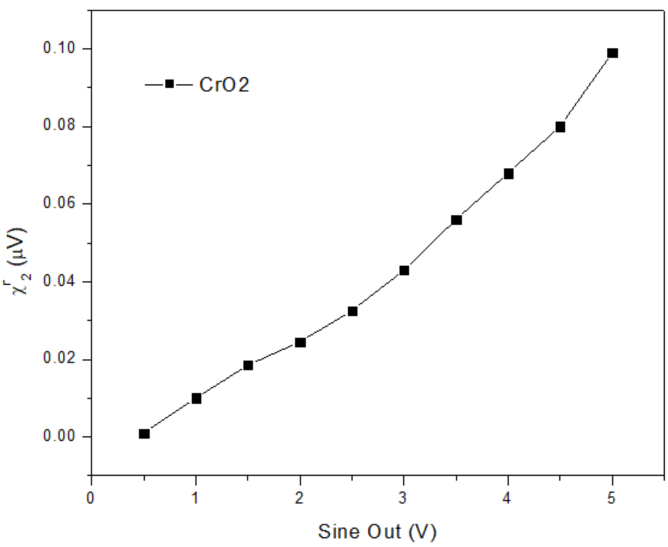

Figure 2.12: CrO_2, Second Harmonic Real Part : AC-χ vs Applied Magnetic Field (signal measured v sine-out)

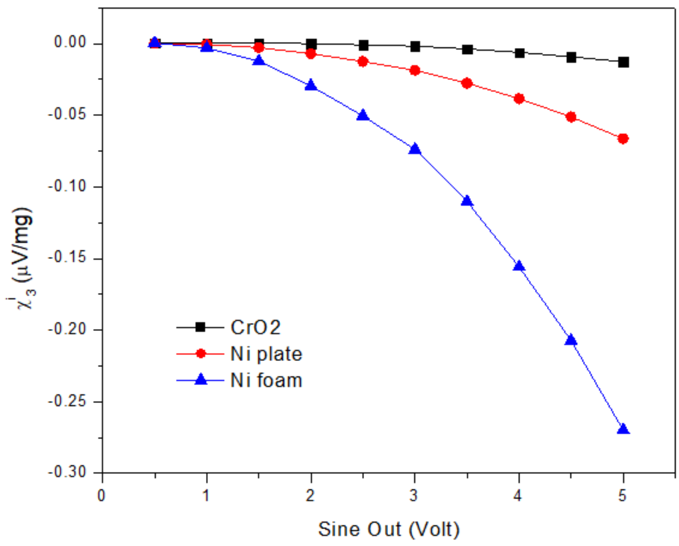

Figure 2.13: CrO_2, Ni plate & Ni foam, Third Harmonic Imaginary Part : AC-χ vs Applied Magnetic Field (signal measured v sine-out)

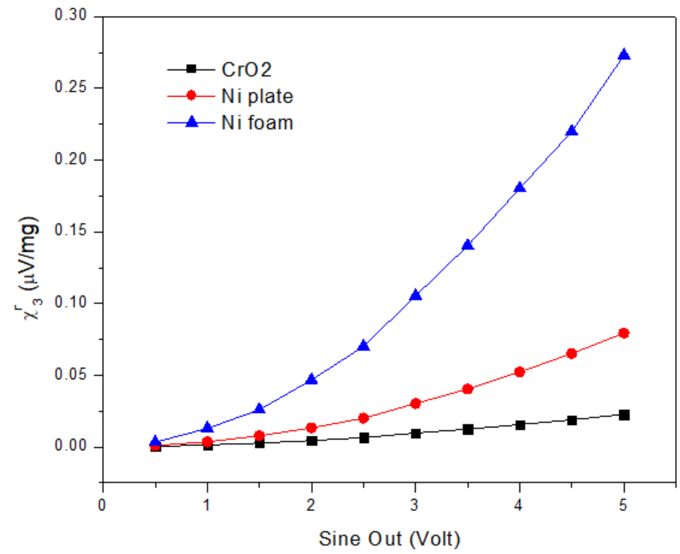

Figure 2.14: CrO_2, Ni plate & Ni foam, Third Harmonic Real Part : AC-χ vs Applied Magnetic Field (signal measured v sine-out)

Here, we can see in the graphs shown in figures above that $CrO2$ gives out less signal than both Nickel plate and foam, except for the imaginary part of the third harmonic. These signals are again in the order of $\mu V/mg$. The nature of the data is same as the Nickel, that is linearly increasing for the first harmonic, but exponential for the third harmonic, decreasing for the imaginary part and increasing for the real part.

For the second harmonic data of CrO_2, we see an almost linearly decreasing trend for the imaginary part but a linearly increasing one for the real part, where the signal is of the order of μV.

2.4.2 CrO_2 Run at a Fixed Low Temperature for First, Second and Third Harmonic

Just like the run at RT, we did a run for the signal measured vs the sine-out value, which corresponds to the ac-χ vs the applied magnetic field here but at a fixed lower temperature, around 153 K. This temperature is achieved by keeping the coil in a thermocol container filled with liquid nitrogen. Here we can compare the run at room temperature and low temperature.

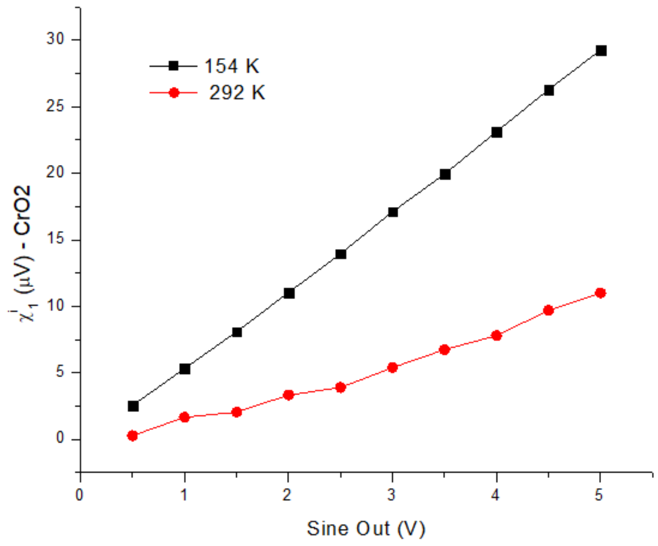

Figure 2.15: CrO_2, at LT & RT, First Harmonic Imaginary Part : AC-χ vs Applied Magnetic Field (signal measured v sine-out)

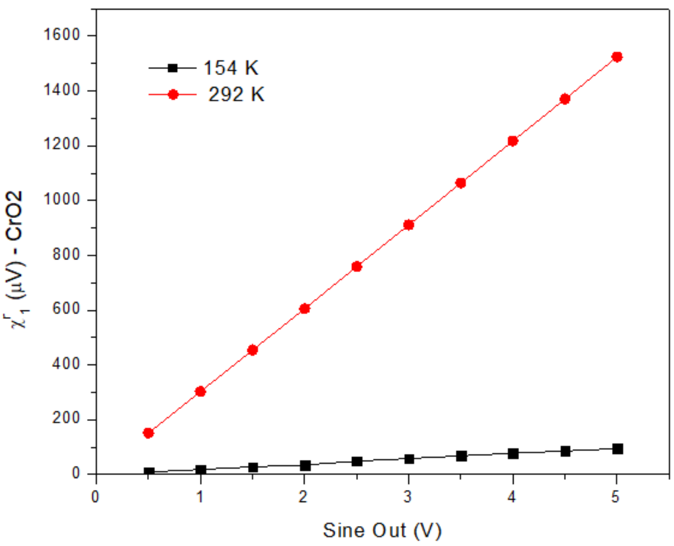

Figure 2.16: CrO_2, at LT & RT, First Harmonic Real Part : AC-χ vs Applied Magnetic Field (signal measured v sine-out)

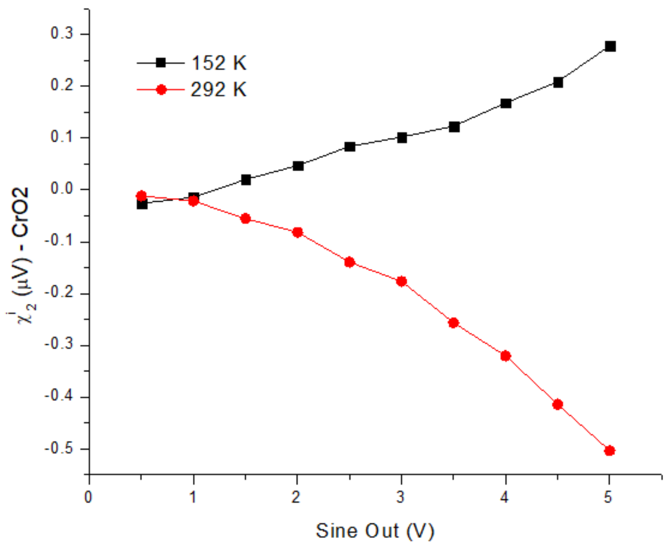

Figure 2.17: CrO_2, at LT & RT, Second Harmonic Imaginary Part : AC-χ vs Applied Magnetic Field (signal measured v sine-out)

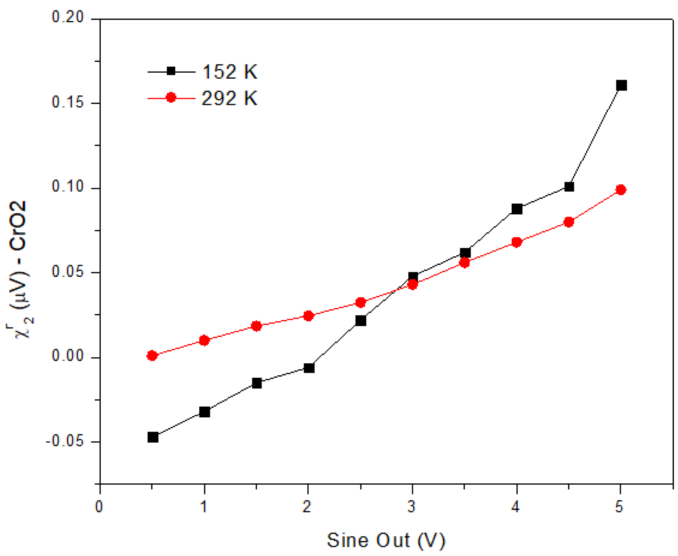

Figure 2.18: CrO_2, at LT & RT, Second Harmonic Real Part : AC-χ vs Applied Magnetic Field (signal measured v sine-out)

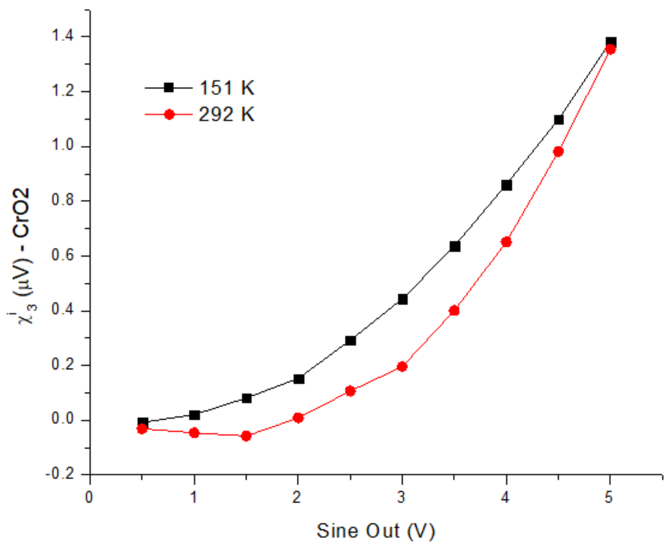

Figure 2.19: CrO_2, at LT & RT, Third Harmonic Imaginary Part : AC-χ vs Applied Magnetic Field (signal measured v sine-out)

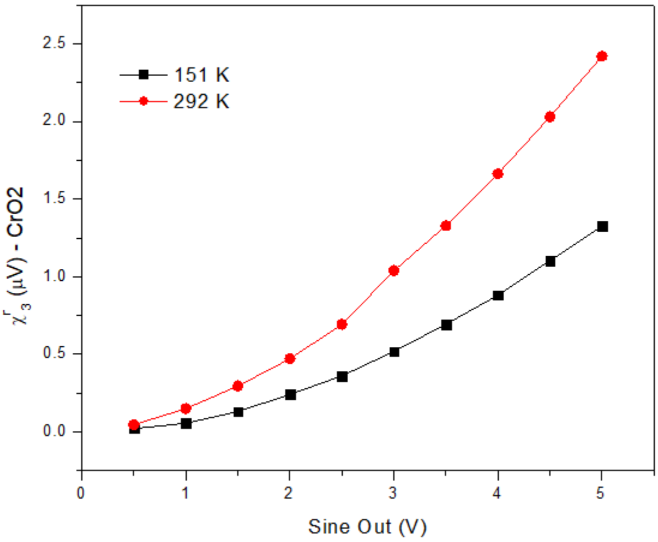

Figure 2.20: CrO_2, at LT & RT, Third Harmonic Real Part : AC-χ vs Applied Magnetic Field (signal measured v sine-out)

From all the graphs on LT and RT we have for CrO_2, we can say that

- **First harmonic :** For the imaginary part we get larger signal on LT than RT, but in real part, larger signal is observed for RT.
- **Second harmonic :** For imaginary part, again we observe larger signal on LT where it is increasing while the RT one decreases, but we observe a crossover in real part where LT is leading the later part.
- **Third harmonic :** Just like first harmonic, LT gives larger signal for the imaginary part meanwhile RT gives more signal for the real part

The higher signal received at RT for real part can accounted to the fact that since the Curie temperature for the CrO_2 is around 393 K, and the more we move towards the direction of it, the signal will slightly rise.

Chapter 3

Construction of the Heater for the High Temperature AC-χ Set Up

In this chapter, we will talk all trials to making a heater and a sample rod suitable for high temperature measurements. This sample rod should be compatible with existing glass inserts for ac-χ set up. Our primary goal is to investigate the linear and non linear magnetic susceptibilities act in the vicinity of a ferromagnetic to paramagnetic transition temperature for the ferromagnets. By high temperature, we are referring to the temperature at least upto 700 K or 800 K. For this, we will need a heater that is compatible with existing double walled ac-χ insert made of quartz.

For this purpose, our test sample is Ni, which is a well known elemental ferromagnet with Curie Temperature $\sim$ 627 K. Measurement of linear and non linear susceptibilities in the vicinity of T_C in this sample would enable us to compare our data with that existing in literature[22] and also enable us to explore the effect of morphology, especially in the nature of higher harmonic susceptibility, which is expected to show a cross over in sign in the vicinity of the transition temperature.

3.1 Choice of Materials for Sample Rod and Heater

In this section we will go through what material we acquire for making the heater and the sample rod.

3.1.1 A General Sample Rod

Sample rod consists of two parts. First part is a sapphire tube (length about 10 cm, diameter about 5 mm) or a ceramic tube (length about 20 cm, diameter about 5 mm). On the sapphire (or ceramic tube) the heater wire is wound and a temperature sensor

(PT 100) is attached at the one end. The sample can be mounted at the other end of the sapphire (ceramic tube). This assembly is attached to a is attached to a 1 meter glass tube or a 1 meter SS tube (or a 1 meter quartz tube), through which the wire connections are hermetically taken out.

3.1.2 Heater Wires

Two types of heater wires have been tested for high T set up. First is Kanthal, D grade. Kanthal wire is a ferritic iron-chromium-aluminium alloy (FeCrAl alloy) which is suitable for temperatures up to 1300 degree Celsius. This alloy has a high resistivity and a very good oxidation resistance. It has a resistivity around 1.45 $\Omega\ mm^2$/m at RT[14]. It is desirable to have a non magnetic heater wire, that does not interfere with magnetic signals during measurement of ac susceptibility. However, Kanthal are magnetic up to a temperature of approximately 600 degrees Celsius, which is its Curie temperature.

Trials were also made with Nichrome, which is an alloy of nickel and chromium (80 percent Ni, 20 percent Cr) and can reach temperature up to 1200 degree Celsius. Moreover, it also possesses good resistance to oxidation, good electric resistance and high-temperature capability.

3.1.3 Adhesive

We have used two types of high temperature adhesive. First is a 'Zircobond-II Ceramic Adhesive Cement', a type of cement that is usually used at higher temperature a furnace, which was purchased locally. It is typically used in 2:1 mass ratio of the cement powder and the liquid precursor to form the paste. It can work upto around 1250 degree Celsius.

Second high temperature adhesive is magnesium oxide powder (MgO), which can be made in the form of paste using ethanol. We can use it by making a soft dough of this magnesium oxide powder and ethanol.

3.2 Heater Winding

We made trials by winding Kanthal and Nichrome wires in non inductive fashion. For non inductive winding, wire is folded from the middle prior to winding. For reaching the desired temperature (above the curie temperature of Ni) we also used commercially available heater wires, which was purchased locally, customized to the best of our needs.

Figure 3.1: PRT - PT 100 with ceramic coating

Figure 3.2: Sapphire tube for heater base

3.3 Trials on Heater Winding

The development of a custom high-temperature heater suitable for AC susceptibility measurements required careful iteration across several design parameters including wire gauge, length, resistance, thermal contact, and magnetic compatibility. Many attempts were made, each addressing specific challenges encountered in previous efforts. This section presents a comprehensive narrative of the sequence and outcomes of these trials.

In our **first attempt**, we used 40 cm of Kanthal wire with a thickness of 24 SWG, giving a resistance of 14.8 Ω. The wire was wound directly onto a sapphire tube (6.6 mm ID, 10 cm length), and a diluted high temperature cement paste was applied to fill gaps between the wire and tube to improve adhesion. After allowing it to dry for a day, a platinum resistance thermometer (PRT) was mounted using copper wiring. However, upon testing with increasing current from 1 mA up to 0.5 A, no observable heating was recorded. This failure was attributed to insufficient thermal contact between the Kanthal wire and sapphire's surface.

Before next attempt, inspired by the use of GE varnish in low-temperature setups, a cement layer was applied to the wire before winding, with the hope that once dried, it could be peeled and reattached. However, the cement proved too brittle and cracked upon attempting to wind the wire onto the sapphire tube. This demonstrated the incompatibility of this method for rigid adhesives on curved surfaces.

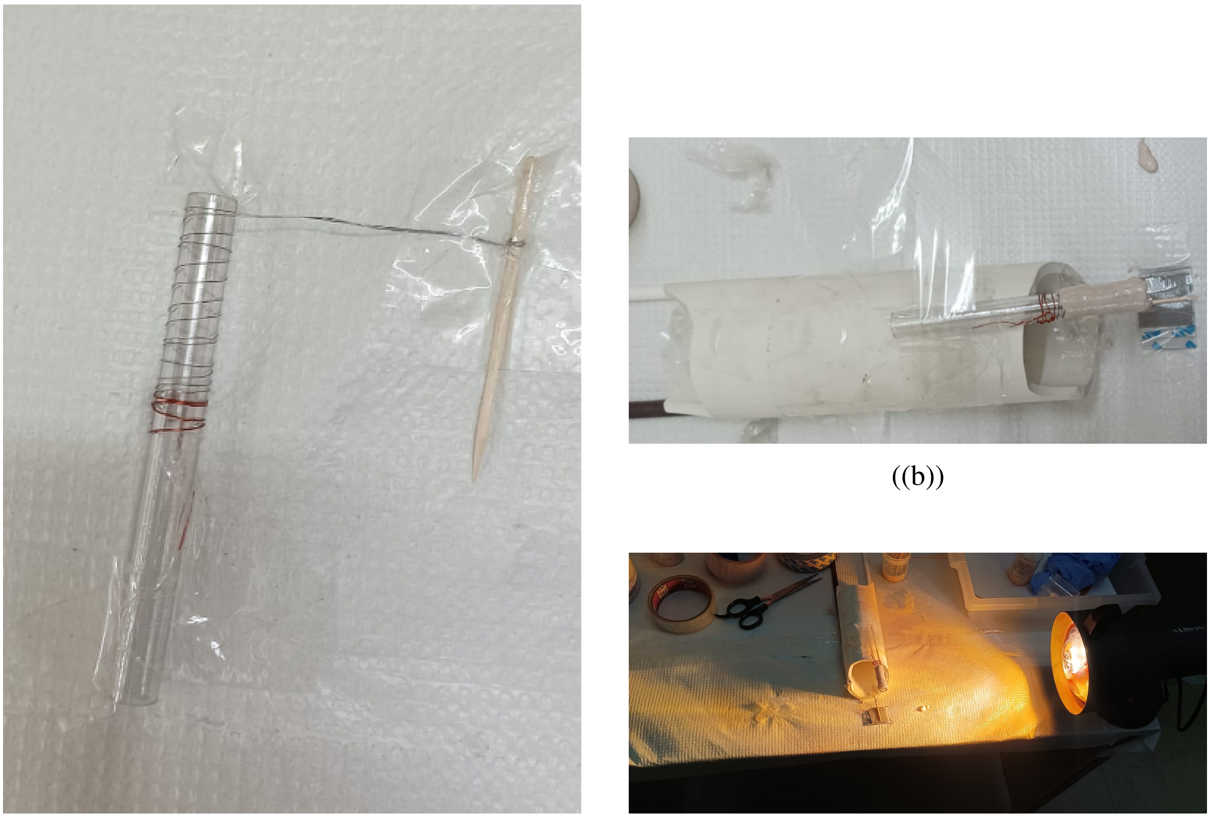

((a)) ((b)) ((c))

Figure 3.3: First attempt : (a) Kanthal wire in non inductive winding on sapphire tube, (b) High temperature cement applied on the the heater, (c) Applied cement drying under IR lamp

Figure 3.4: Drying cement applied on straight heater wire by using IR lamp

In the **second attempt**, we switched to a thinner Kanthal wire of 33 SWG to increase the resistance and allow for better heating. A length of 118 cm yielded 25 Ω resistance. With this configuration, and using a DC sourcemeter as a power source, we achieved a maximum temperature of 381 K before reaching the compliance limit of the current source. This demonstrated partial success and validated the strategy of increasing resistance via thinner and longer wire.

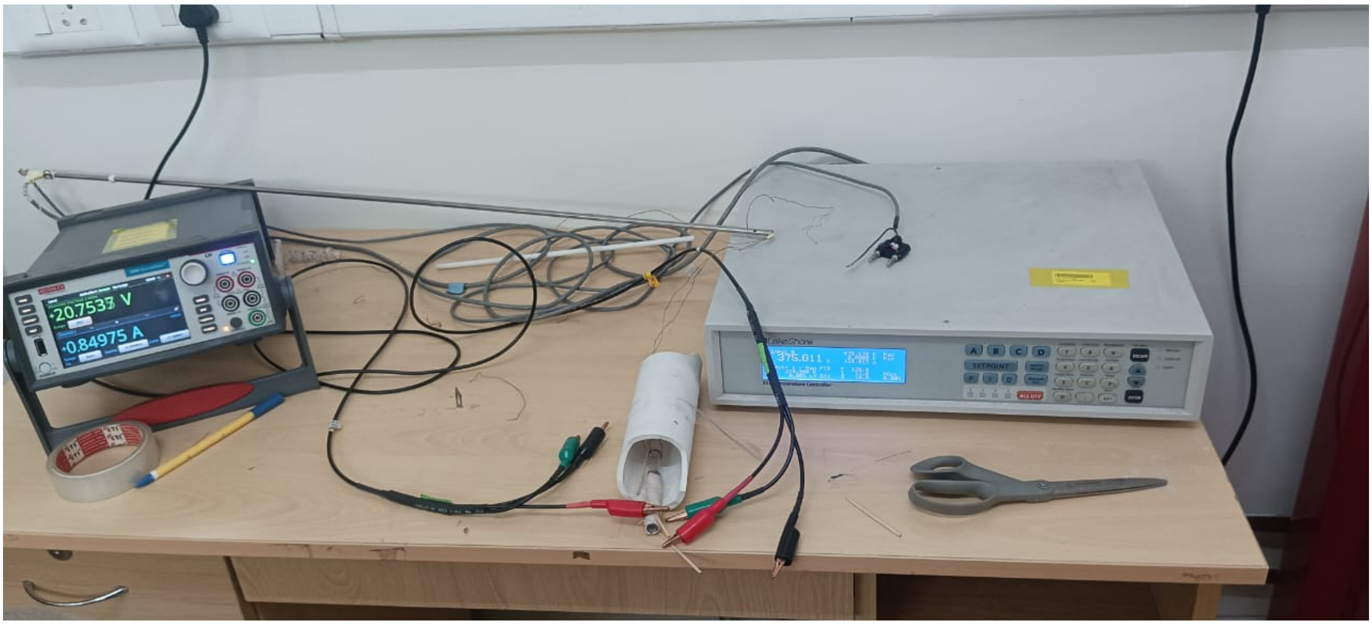

Figure 3.5: Third attempt : heater being tested with DC sourcemter and Lakeshore temperature controller

This **fourth attempt** is similar to the last one, where the difference being that for increasing the resistance, we have increased the length of the wire to 118 cm, making the resistance to be 36 Ω. This time we used Lakeshore temperature controller as the source. In this attempt, we observed a slightly higher temperature, 424 K, before the compliance of the source was reached.

Building on this, the **fourth attempt** used 188 cm of the same wire to increase the resistance further to 58 Ω. To accommodate this length, the wire was divided between a sapphire tube and a ceramic rod. No cement was used. A dimmerstat served as the power source, but due to incorrect labelling on the device, excessive voltage led to the burning of the heater wires before any temperature measurements could be made.

In the **fifth attempt**, a thinner 36 SWG Kanthal wire was used to further boost resistance, now reaching 96 Ω across 225 cm. This wire was wound inductively on a ceramic rod without any adhesive, and a dimmerstat was again used. Unfortunately, the heater wire burned out at 210 V, and the maximum temperature achieved was just below 100°C. This highlighted the fragility of very thin wires under high voltage stress without protective coating.

Figure 3.6: Fourth attempt : heater wires at one end got burnt due to excessive voltage applied

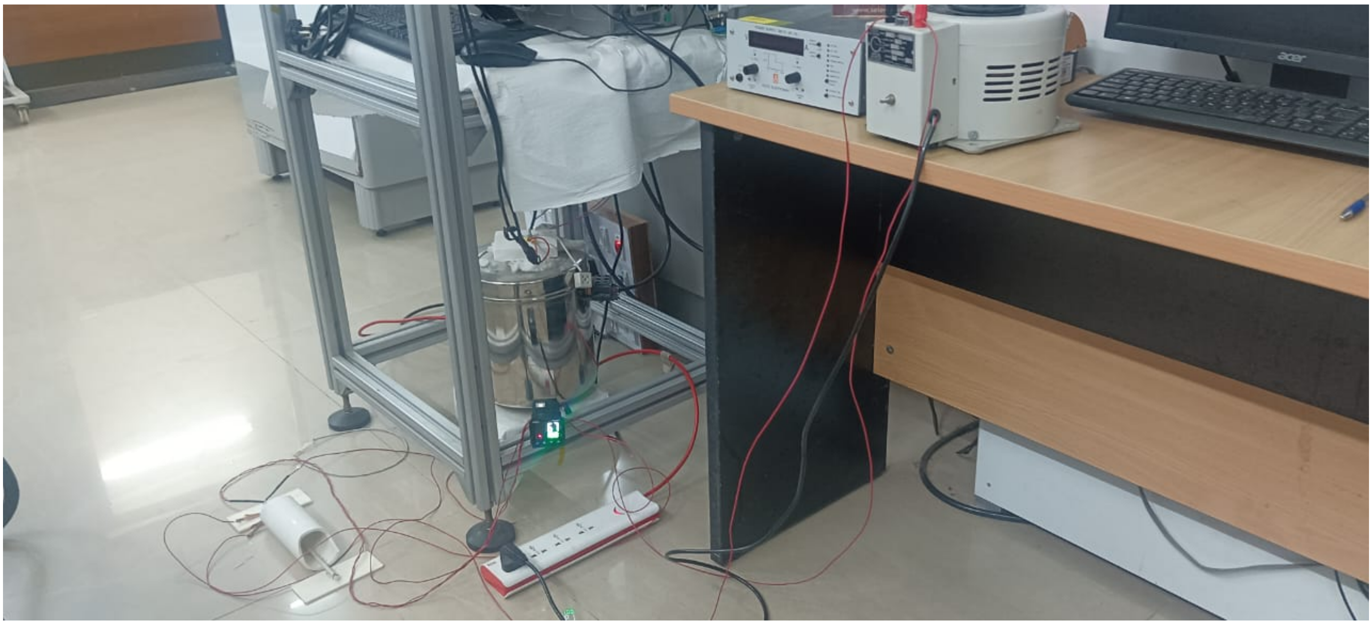

Figure 3.7: Fifth attempt : Heater being tested with PID temperature controller & a dimmerstat

For the **sixth attempt**, we retained the 36 SWG wire and increased its length to 300 cm to push resistance up to 133 Ω. The wire was wound non-inductively using ceramic beads on a ceramic rod and powered via a Lakeshore temperature controller. The system reached 333 K before the temperature began to drop, suggesting inadequate thermal contact or issues in PID tuning. These results motivated further refinement in both winding method and thermal interface.

Figure 3.8: Sixth attempt : Kanthal wires wound non inductively with the help of ceramic beads

In the **seventh attempt**, we reverted to 33 SWG wire (95 Ω) while keeping the non-inductive winding approach with ceramic beads. Cement was applied on top for stability. While the heater performed better, reaching up to 442 K, the temperature eventually declined again—indicating persistent thermal losses or delamination. It became evident that cement was not the ideal thermal or mechanical adhesive for this configuration.

Given the limitations of hand-wound setups, the **eighth attempt** involved procuring a commercial custom-made heater. It consisted of Nichrome wire wound inductively, precisely on a ceramic rod using automated machinery and encased in an Inconel 800 sheath. This design delivered a resistance of 230 Ω and achieved temperatures of 554°C at 220 V with a dimmerstat. While the performance was excellent, the weak magnetic nature of Inconel 800 posed a problem for sensitive susceptibility measurements.

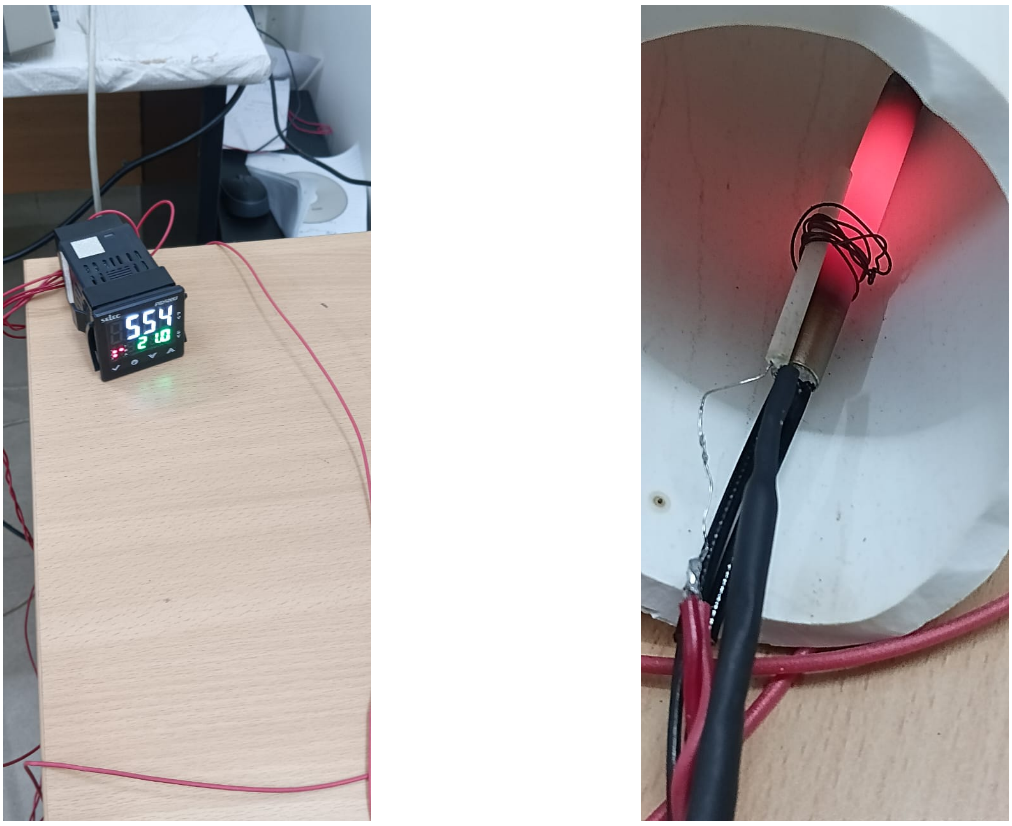

Figure 3.9: Eigth attempt : heater with inconel 800 casing tested with PID temperature controller and dimmerstat

To evaluate compatibility with our control electronics, the **ninth attempt** tested the same commercial heater with the Lakeshore temperature controller. It successfully reached $\sim$550 K, the upper bound of the controller's PT 100 sensor curve, confirming electrical and thermal suitability of the heater.

Finally, in the **tenth attempt**, we requested a version of the same custom heater without the Inconel 800 casing to eliminate unwanted magnetic background. Testing this modified heater with a dimmerstat showed it could reach 410°C at 110 V, making it well-suited for our experimental requirements. This heater was ultimately selected for integration into our AC susceptometer.

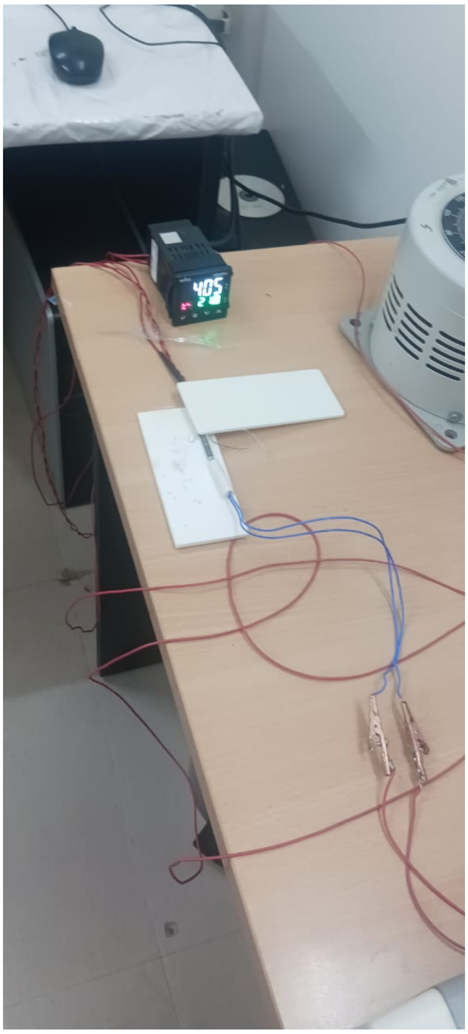

Figure 3.10: Tenth attempt : Heater being tested with PID temperature controller and a dimmerstat without the inconel 800 casing this time

Table 3.1: Heater specs for various trials

No.	Length(cm)	SWG	Res.(Ω)	Wound On	Wire	Max Temp.	Source	Comp.
1	40	24	14.8	Sapphire	Kanthal	-	Lakeshore	50V
2	80	33	25	Sapphire	Kanthal	381 K	DC Sourcemet.	20V
3	118	33	36	Sapphire	Kanthal	424 K	Lakeshore	50V
4	188	33	58	Cera.+Sapp.	Kanthal	-	Dimmerstat	220V
5	225	36	96	Ceramic	Kanthal	372 K	Dimmerstat	220V
6	300	36	133	Ceramic	Kanthal	333 K	Lakeshore	50V
7	300	33	95	Ceramic	Kanthal	342 K	Lakeshore	50V
8	-	-	230	Ceramic	Nichrome	827 K	Dimmerstat	220V
9	-	-	230	Ceramic	Nichrome	560 K+	Lakeshore	50V
10	-	-	230	Ceramic	Nichrome	683 K+	Dimmerstat	220V

3.4 Final Version

Based on the outcome of these trials, final version of heater assembly was made using commercial heater. Now for the thermal contact, we used magnesium oxide. However, we decided to give up on this for the time being and to go for the nichrome based heater inductively wound on a small ceramic rod on which we tested our last few heater runs. This is wound on a ceramic rod, which has a resistance around 70 Ω. One key reason behind choosing this was difficulty in going for non inductive winding on sapphire because of slipping and the difficulty in maintaining proper thermal contact.

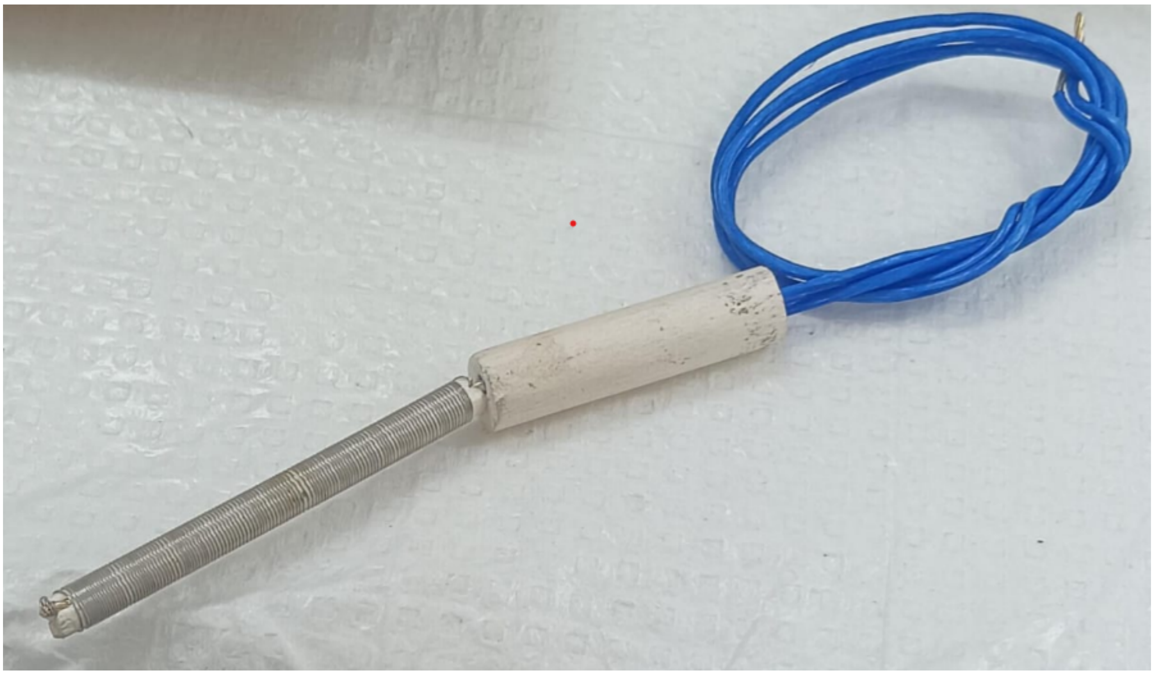

Figure 3.11: Commercial heater used in final run : Nichrome wire wound on a ceramic tube, inductively, with a resistance of around 70 Ω

Chapter 4

Assembling the High Temperature AC-χ Set Up

In this chapter we will discuss how we have built our set up for the high temperature ac-χ set up, from what parts we have used to for what purposes. We will talk about the different parts involved like sample rod, sample holder, inner dewar, outer dewar, LN2 dewar, heater, vacuum parts, secondary coil, primary coil and the base to hold it in.

4.1 Coils

The primary coil wound on a hylum former is same as the one used previously for our preliminary runs in chapter 2 [7], shown in image 4.1(a). The secondary coil-set is replica of the one described in the pre existing LT ac susceptometer in the lab[26], and this one is wound on a quartz tube. However, one of its secondary was damaged and hence it was wound again using a coil winding machine during the course of this project as shown in image 4.1(b)

Table 4.1: Specifications of Coil Windings

Component	**Number of Turns**	**Resistance (Ω)**	**Dimensions**
Primary Coil	1380	85	Length of winding: 150 mm
Secondary Coil 1 (Rewound)	3512	423	Length of winding: 15 mm
Secondary Coil 2 (Original)	3523	425	Length of winding: 15 mm

((a)) Primary coil

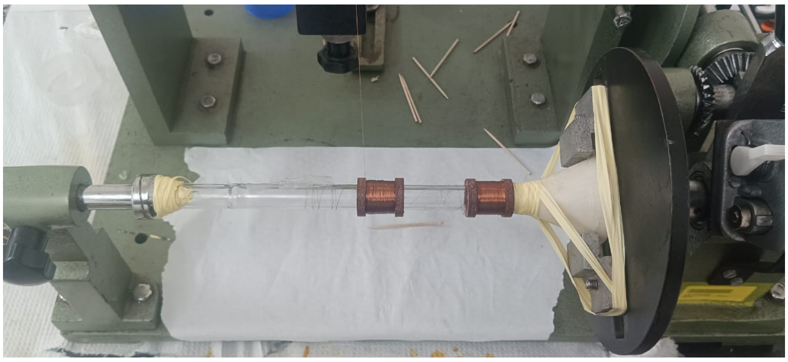

((b)) Secondary coils

Figure 4.1: Coils for the HT ac-χ set up

4.2 Vacuum Insulation Dewars

Vacuum insulation dewars are double-walled containers with a vacuum between the inner and outer vessels to drastically reduce heat transfer. The vacuum layer effectively minimizes conduction and convection, maintaining thermal stability. This insulation is essential for precise temperature control in high-temperature measurements. It also helps reduce power consumption and protects the setup from external temperature fluctuations. In next subsections, we will talk about their specifications.

4.2.1 Outer Dewar

The outer dewar is a glass tube of an original length of 80 cm with one side sealed and other opening mouth of size KF25. We cut it out from one end for about 25 cm and fused the glass tube on which the secondary coils are wound, which has a length of around 22.5 cm, making the total length to be around 77.5 cm.

4.2.2 Inner Dewar

The inner dewar is a glass tube of an original length of 1 m. We sealed its one end and fused a glass KF 16 at the other end, making the total length to be around 112 cm.

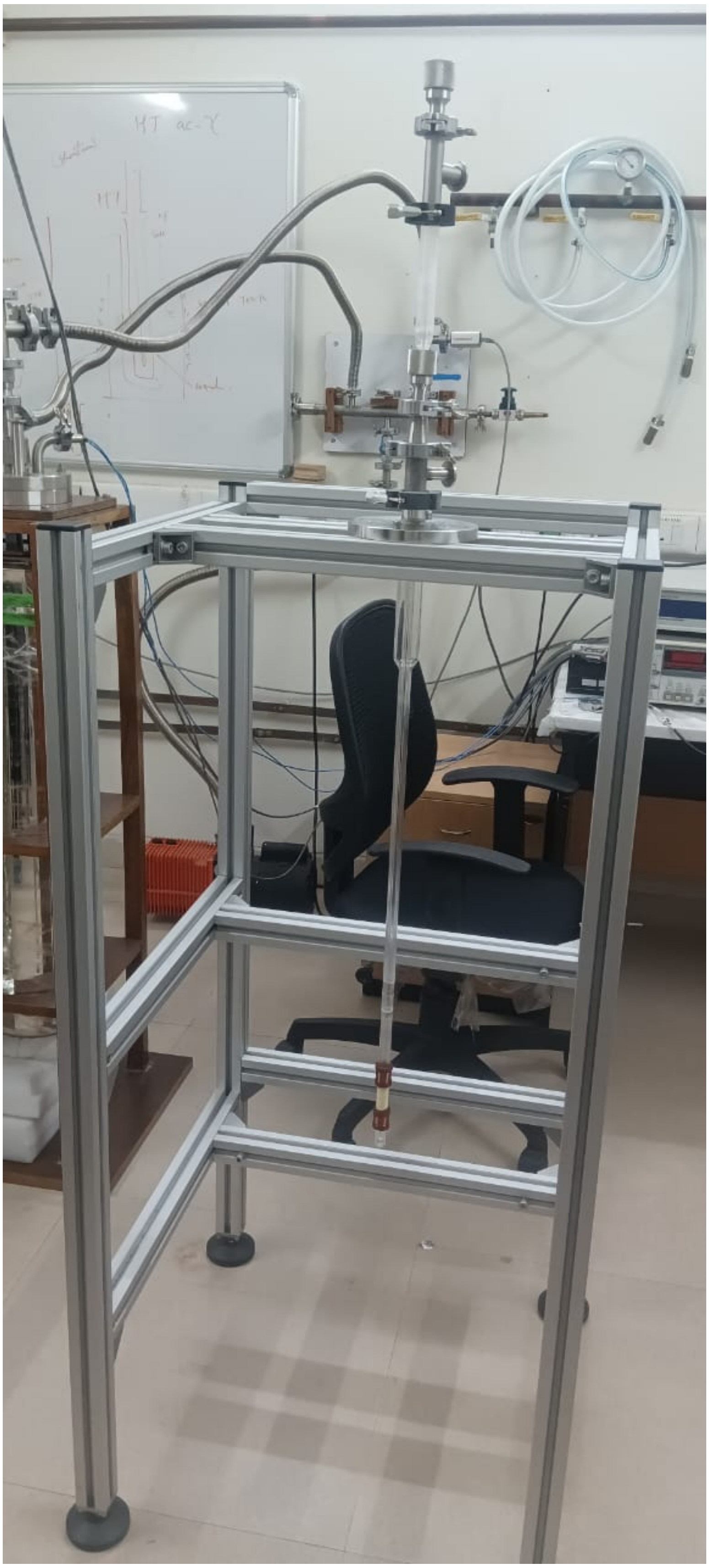

Figure 4.2: Base of the final assembly with outer dewar hanging with the help of coupler and a metal plate with KF 25 opening on both sides, and inner dewar is inside the outer dewar with the help of wilson seal

4.3 The Sample Rods

We made a couple of sample rods for the use in the high T ac-χ set up. The general design of the sample rod consists of a hollow one meter tube, made of SS or glass. One end of this tube is hermetically sealed with Torrseal and carry connection wires. The other end of the tube is connected to either a sapphire or a ceramic tube of about 15 or 20 cm length. On this smaller part, the heater, temperature sensor and the sample is placed. The resistance of the heater is about 70 Ω, and the PRT (PT-100) sensor is used for measuring temperature.

For our final sample rods, we tried different ideas, but mainly the following three -

4.3.1 Sample Rod 1

It is a full glass tube of length around 100 cm. At the end of this tube, another glass tube of 15 cm length is attached, that contains heater and PRT. A test run was made using this sample rod to check the maximum temperature reached when PRT and heater are anchored to the glass tube using copper wires, under vacuum conditions. With this rod, we first wanted to see the maximum temperature it can achieve, where our heater and sensor are in contact with the glass's surface. We put this inside our hanging inner dewar, with the help of couplers and wilson seal, under vacuum conditions, and the highest temperature we achieved was around 650 K, which is just above our required nickel's T_c i.e. 627 K. After which our heater burned out. We first tried it with Lakeshore temperature controller as the heater source, but could only reach around 610 K, but with the help of dimmerstat we were able to reach around 650 K before the heater was burnt.

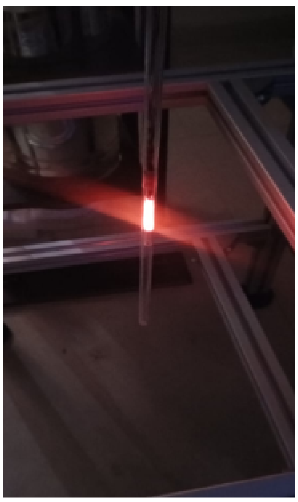

Figure 4.3: Sample Rod 1 : Testing our heater with which reached $\sim$ 650 K, under vacuum condition

4.3.2 Sample Rod 2

Here, we used two sapphire tubes of different diameter, with thinner one (OD 4.5 mm) attached with glass rod on one end and with a slightly thicker sapphire tube (ID around 5 mm). All the attachments are done with the help of copper foil and wires, with heater inside the bigger one while sensor half inside each sapphire tube. With this arrangement under vacuum, we could reach maximum 480 K.

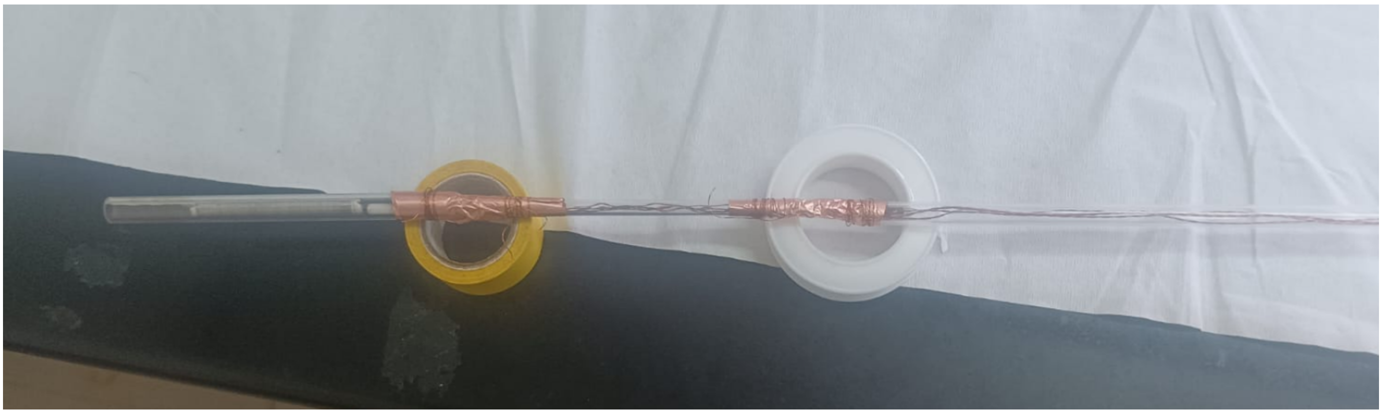

Figure 4.4: Sample Rod 2 : Sapphire tubes mounted at the end of glass rod with the help of copper foils and wires, and heater with sensor inside the sapphire tube

4.3.3 Sample Rod 3

For our third and the final version that we have used for our measurement, we have used a glass tube of 1 meter length. At the end of this glass tube, a ceramic tube is attached that contains heater, sensor and the sample. This ceramic rod (OD 4 mm) is inserted in it for providing decent sturdiness to the rod and then heater, sensor and the sample mounted on the ceramic rod, with some gap between the heater and the sample to avoid getting any signal from the heater itself. This way under vacuum we were able to reach maximum of around 750 K, and then we took our data with this sample rod only.

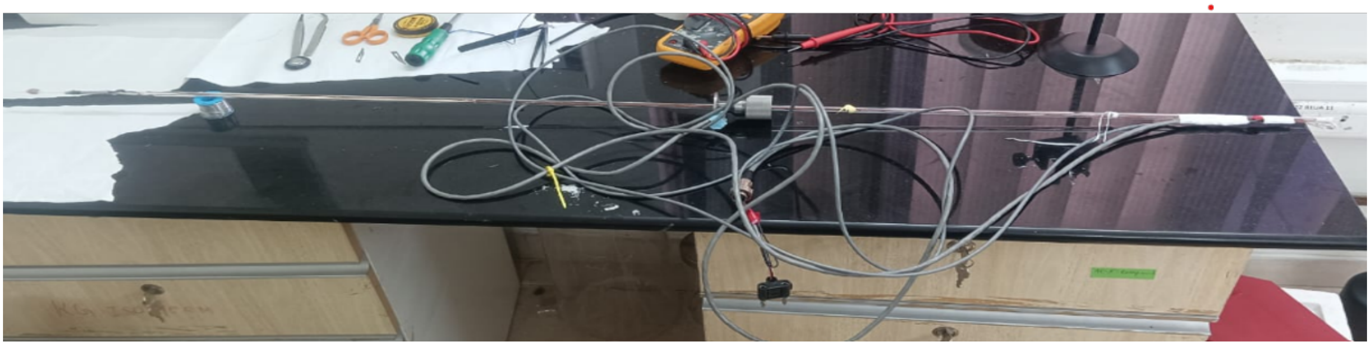

Figure 4.5: Sample Rod 3 : A ceramic rod is inserted in our glass tube as base with heater, sensor and sample mounted on the ceramic rod

4.4 Assembling Components & Making Connections

A metal plate with an KF25 opening on each side is mounted on an aluminium framework, with a hylum plate's support. Then on the lower end of this metal plate, we attached our outer dewar which has the secondary coil on it. Then on the other end, we attached a T shaped KF 25 pipe with an outward opening for vacuum evacuation between the outer and inner dewar. Wilson seals were also used for rod insertion and to maintain vacuum in the space between dewars and sample rod.

Each part of the secondary coil is connected in the series opposition. For primary coil, a 1 Ω resistor is also connected one one end and then all the ends are connected to the respective points in the lock in amplifier for taking the readings. We have used a Stanford 850 LIA for our purpose. Dimmerstat is then connected to the heater wires and PRT sensor to the Lakeshore temperature controller for the temperature measurement.

After this, we used another hylum plate hanging from the first hylum plate with the help of two small hylum rods of length around 10 cm with screws attached on ends, on which we hung our primary coil with the help of two similar hylum rods of length 60 cm. Some small hylum pieces like a hook was inserted between primary and secondary coil to keep it sturdy.

For this test, we did not use the inner dewar because of the unavailability of space while inserting our sample rod, but we will use it in our future runs for providing better thermal insulation for our coils.

We can see how it looks in figure 4.6

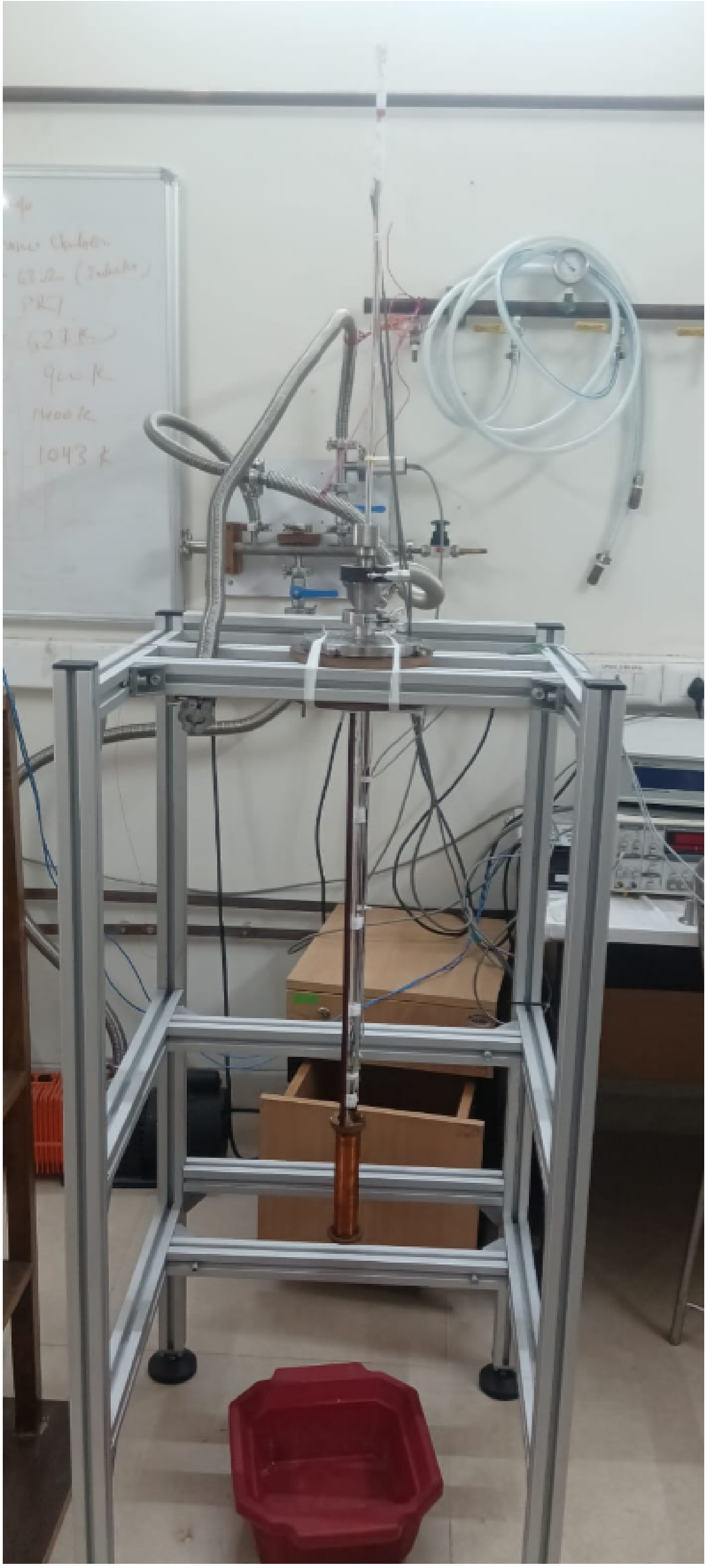

Figure 4.6: Primary coil hanging with the support of hylum rods and plates fixed to the aluminium framework, with secondary coil inside

Chapter 5

A Fast Temperature Scan for Ni Foam and The Transition At T_C

In this chapter we will talk about how we assembled the entire set up and took our measurements.

5.1 Sample

For our final sample, we used a Nickel foam, which is a Sigma Aldrich sample. The sample is in the form of a flexible plate, which is folded in the form of concentric tubes, such that it fits reasonably well inside one end of the ceramic tube. The mass of the sample used for this test run is sample is 115.5 mg.

5.2 Methodology

We have connected our PRT sensor with the Lakeshore temperature controller and the heater with the dimmerstat. The inner glass insert containing the sample rod is evacuated and the vacuum is about 7.7 μBar. Full assembled set up can be seen in the figure 5.1

Then we connected our primary coil with the sine out part of the LIA. We will work in A-B mode. So we will be doing our run with fix sine out value of 5 V, which will correspond to an oscillating applied magnetic field $\sim$ 6 Oe. Reference frequency is set at 133 Hz, time constant at 300 ms, and manual reserve at 36 dB.

In next step, we will set our phase. For this we take out the clips connected to A-B mode and put it across the 1 Ω resistor connected on one end of the primary coil, and then we auto phased it from LIA. At this point, the the angle of phase, ϕ is 175.535 degree, where our current value across the resistor is 36.383 mA.

Now we slowly insert our sample rod inside the secondary coil, till it gives out maximum signal while being in the first secondary coil. This will be the mark from where we will take our readings. So now we mark this point on the sample rod with a marker and teflon.

Figure 5.1: Final High Temperature AC - χ Set Up with Labelled Components

5.3 Measurements

Our first step here would be to measure the offset, for which we will pull our sample rod slightly outside such that our sample is out of the coil, and now we measure our offset, and their values are as in the table below -

Table 5.1: Offset Measurements for the High Temperature AC - χ Run

Susceptibility Component	**Real Part**	**Imaginary Part**	**Uncertainty**
χ_1 (First Harmonic)	-0.206 mV	-0.0380 mV	–
χ_2 (Second Harmonic)	0.000 µV	0.000 µV	±30 nV
χ_3 (Third Harmonic)	0.03 µV	0.03 µV	±20 nV

Now sample rod is inserted till the maximum signal point marked earlier for final measurements. We will be taking χ_1 data at 5 and then 10 mV sensitivity, and χ_3 data at 500 μV sensitivity. The curie point of Ni is $\sim$ 627 K and our aim is to take ac-χ data not only in the vicinity of the transition but also in the paramagnetic region. Hence we used dimmerstat, instead of lakeshore temperature controller. Using dimmerstat, maximum temperature achieved is higher as demonstrated in the previous chapter. However, unlike lakeshore, it is not possible to take temperature controlled data using dimmerstat. Hence in this run data is taken manually in one scan of a temperature during heating.

We start our measurement from 297 K, then from 300 K, we took initial measurements at around 20 K interval, till 500 K, after which we started taking data at an interval of 10 K till 600 K, after which we keep on reducing our interval to take better measurements. We also noticed a slight change in pressure under vacuum because of degassing in the heating process.

It is to be noted that this is a fast scan in which data is recorded while heating, without controlling the temperature. For such a scan, as temperature rises, the difference between the sample temperature and the sensor keeps increasing. The sensor is close to the heater and both sensor and heater are about 3-4 cm away from the sample location. This leads to a significant lag between the actual sample temperature and the sensor. However the purpose of this run is to measure ac susceptibility in the vicinity of the Curie temperature, which should be marked by a large change in its magnitude, even though there would be a shift in the temperature axis due to the lag between the sensor and the actual sample temperature.

The susceptibility vs T data has been recorded for the real and imaginary part of first and the third harmonic. This is shown in the figures 5.2 and 5.3. In these graphs we could clearly see a transition as we expected in both χ_1 and χ_3.

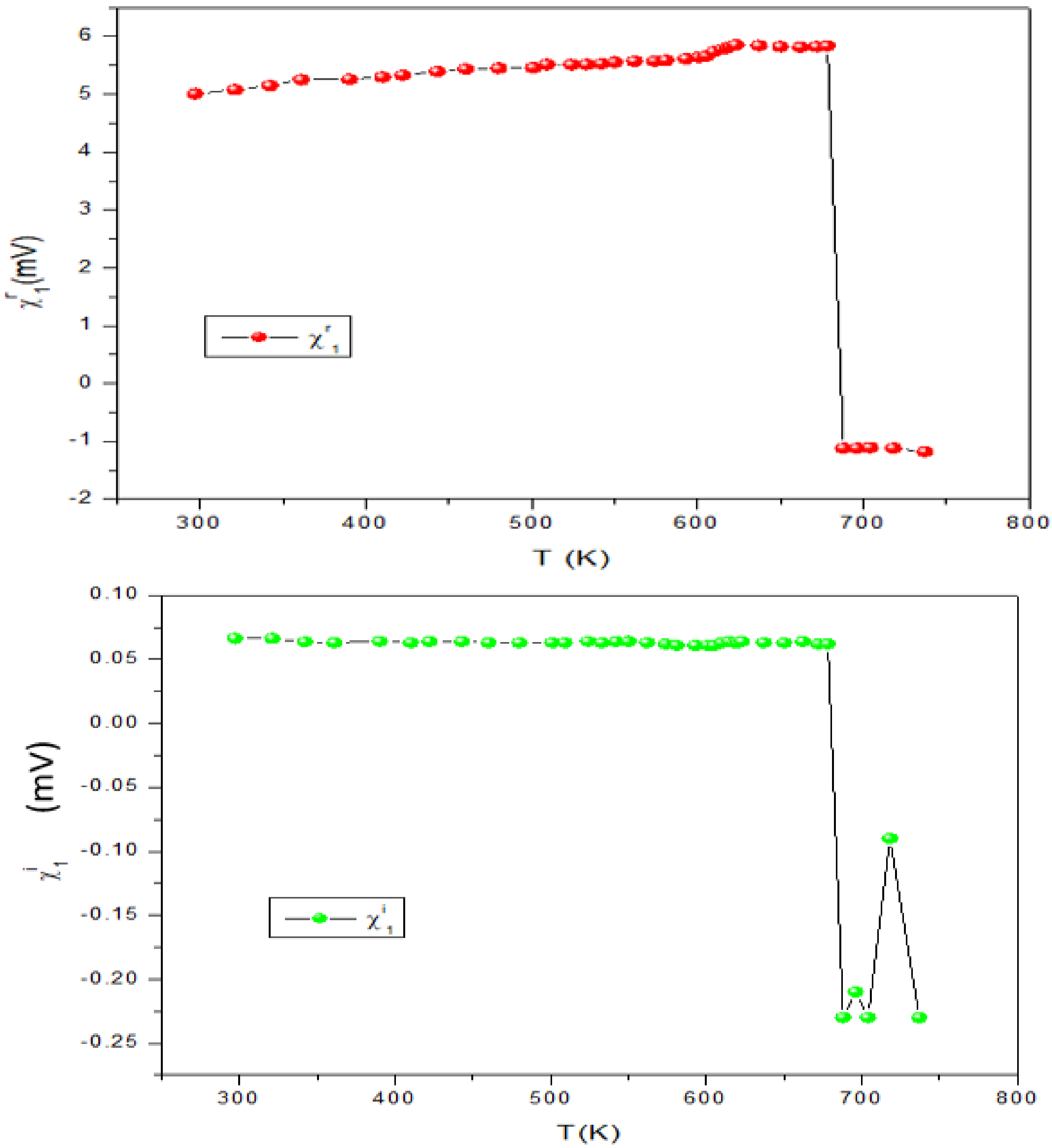

Figure 5.2: Nickel : χ_1 v T (both real and imaginary parts)

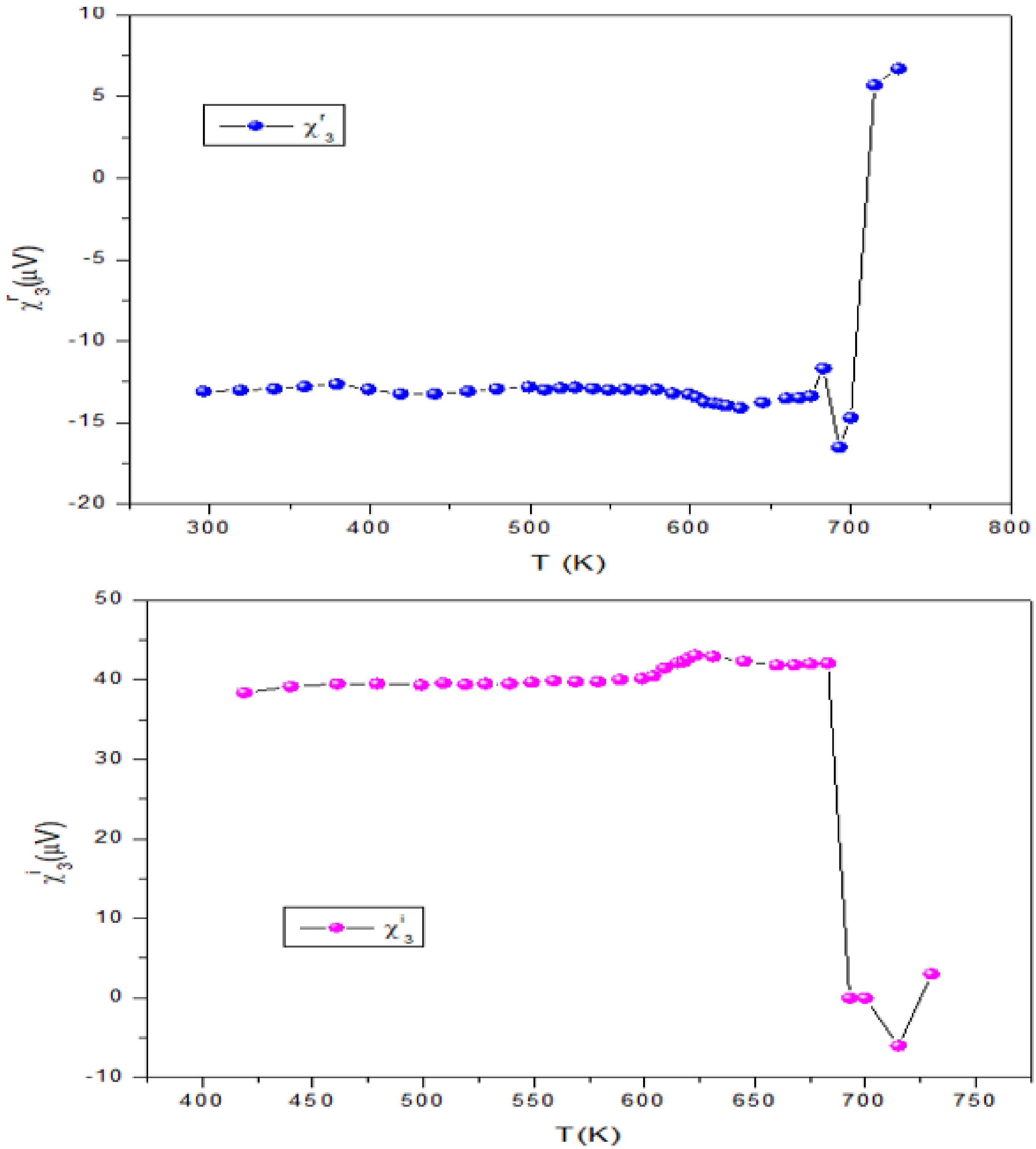

Figure 5.3: Nickel : χ_3 v T (both real and imaginary parts)

5.4 Nickel Transition Data at Higher Temperature: Results & Discussion

In the end, ac susceptibility measurements at high temperature were performed on my set up with a nickel foam sample to investigate its magnetic phase transition near the Curie temperature (T_c). Despite the experimental limitations, including uncontrolled temperature ramps and manual data collection, the results revealed clear transitions in both the first and third harmonics, which are characteristic of the ferromagnetic to paramagnetic phase transition in nickel. The transition temperature observed in our experiment was around $\sim$ 690 K, which is higher than the expected $\sim$ 627 K. This discrepancy can be attributed to the difference between the temperature measured by the sensor, which was placed near the heater, and the temperature experienced by the sample, which was kept 5 cm away to avoid interference from the heater's inductive fields. This temperature gradient between the sensor and the sample suggests thermal contact between the sensor and the sample needs to be improved.

The real part of the first harmonic (χ_1') showed a significant drop as the temperature approached the transition temperature, providing strong evidence of the magnetic phase transition. This drop is a well-known signature of ferromagnetic to paramagnetic transitions, where the magnetization of the material decreases as it crosses T_c. The sharpness of the drop in the real part of χ_1 is particularly notable, as it indicates a well-defined transition between these two magnetic states. This behaviour aligns closely with the data presented in Shirane et al.[22], confirming the expected transition in nickel at high temperatures. However, we could not take reasonable data in the paramagnetic region due to heater related limitation. We are approaching T_C on a heating cycle, i.e. from below T_C (heating from RT, towards 627 K). However present system is not adequate for this high temperature. We would not only need better temperature control but also improvement in sample holder design to investigate critical region for Ni.

In addition to the first harmonic, we also observed the behaviour of the third harmonic (χ_3) during the phase transition. Similar to χ_1, the third harmonic exhibited a transition at approximately the same temperature, characterized by a distinct change in the sign of the signal. This sign change in χ_3 is consistent with the expected response during a phase transition, where the magnetic properties of the material shift. The third harmonic measurement provided further confirmation of the phase transition, supporting the validity of the observed transition in the real part of the susceptibility.

The observed sharp drop in the real part of χ_1 near T_c is reminiscent of the *Hopkinson peak*, a feature commonly seen in ferromagnetic materials at their critical temperature.[11]

The Landau theory of phase transitions provides a useful framework for understanding the observed behaviour. In this context, the order parameter (magnetization) near T_c is expected to exhibit a continuous change, with the free energy expansion revealing a symmetry-breaking transition from the ferromagnetic to the paramagnetic phase.[18] This theory predicts the sharp drop in susceptibility as the system undergoes a phase transition. Moreover, the Ising model, which describes the interactions of spins on a lattice, provides insight into the behaviour of the material near T_c. According to the Ising model, below T_c, the spins are aligned in a ferromagnetic order, while above T_c, they become disordered[29].

Despite some experimental limitations were present, such as temperature control issues, the data obtained show the possibility of measuring magnetic phase transitions at higher temperatures through linear and non linear susceptibility.

Chapter 6

Future Work

These will be the future work on this project on which we would like to focus next -

- **Calibration of the setup:** Precise calibration is essential to ensure accurate susceptibility measurements across temperature ranges. Future efforts will focus on benchmarking the system using standard reference materials and quantifying systematic offsets.
- **Develop a new non-inductive heater using sapphire:** Designing a custom heater with non-inductive winding on a sapphire base will reduce electromagnetic interference and ensure thermal stability at high temperatures. Sapphire's excellent thermal conductivity and electrical insulation make it an ideal substrate for precision heating in susceptibility measurements.
- **Reducing distance between sample and heater:** Minimizing the gap between the sample and the heater will improve thermal response times and reduce temperature gradients. This helps achieve more uniform heating, especially crucial near critical transition points.
- **Improve the mechanical stability of the sample rod:** Mechanical vibrations and shifts in the sample rod can introduce noise and irreproducibility. Reinforcing the rod's stability will ensure more consistent signal detection during long measurement cycles.
- **Replace Lakeshore controller with Eurotherm:** The Lakeshore temperature controller has limitations at high temperatures. Substituting it with a Eurotherm controller can enhance stability, accuracy, and safety in high-temperature operations.
- **Enhance resolution of data near T_c:** Finer temperature steps and extended dwell times near the critical temperature will help better resolve subtle changes in susceptibility. This is crucial for accurately identifying phase transitions and crossover behaviour.

- **Study frequency dependence of χ_1 and χ_3:** The frequency dependent behaviour of χ_1 and χ_3 can reveal relaxation times and dynamic critical phenomena. Systematic frequency scans will be conducted to probe these aspects.

- **Apply the setup to other complex magnetic systems:** The instrument will be extended to study spin glasses, antiferromagnets, and geometrically frustrated systems. These materials often show rich non-linear and frequency-dependent responses.

- **Automate the measurement process for long-duration sweeps:** Long temperature sweeps require stable and continuous data logging. Automating these runs with scripting and remote monitoring will reduce manual effort and improve repeatability.

- **Explore critical exponents at higher harmonics:** Higher-order harmonics such as χ_3 and χ_5 can provide signatures of universality classes and scaling behaviour. This setup will be used to extract critical exponents near phase transitions.

References

[1] A. Aharony, P.C. Hohenberg, D. R. Nelson, and J.M. Stephen. Critical behavior of magnets with random anisotropy. *Physical Review B*, 13(6):2250–2273, 1976.

[2] Neil W. Ashcroft and N. David Mermin. *Solid State Physics*. Harcourt College Publishers, 1976.

[3] A. Bajpai and A. Banerjee. An automated susceptometer for the measurement of linear and nonlinear magnetic ac susceptibility. *Review of Scientific Instruments*, 68(11):4075–4079, 1997.

[4] Stephen Blundell. *Magnetism in Condensed Matter*. Oxford University Press, 2001.

[5] Richard M. Bozorth, E. F. Tilden, and A. J. Williams. Magnetostriction of nickel single crystals. *Journal of Applied Physics*, 38(3):1325–1332, 1967.

[6] Soshin Chikazumi. *Physics of Ferromagnetism*. Oxford University Press, 2nd edition, 1997.

[7] Sayan Debnath. Exploring linear and nonlinear ac susceptibilities in a single crystal of α–fe$_2$o$_3$ around the morin transition, using a home-built ac susceptometer. Master's thesis, May 2022.

[8] Jean-Luc Déjardin, Yuriy P Kalmykov, and William T Coffey. Nonlinear magnetic susceptibility of single-domain ferromagnetic particles. *Physical Review B*, 61(2):1486–1493, 2000.

[9] D. Givord. Magnetic properties—magnetic order. In Joel S. Miller and Marc Drillon, editors, *Magnetism: Molecules to Materials IV*, pages 1–39. Wiley-VCH, 2005.

[10] Ludwig Holleis, Joseph C. Prestigiacomo, Zhijie Fan, Satoshi Nishimoto, Michael Osofsky, Gia-Wei Chern, Jeroen van den Brink, and B.S. Shivaram. Anomalous and anisotropic nonlinear susceptibility in the proximate kitaev magnet -rucl. *npj Quantum Materials*, 6(1):66, 2021.

[11] John Hopkinson. Magnetic and other physical properties of iron at a high temperature. *Philosophical Transactions of the Royal Society of London. A*, 180:443–465, 1889.

[12] D.C. Jiles. Frequency and temperature dependence of hysteresis curves in magnetic materials. *Journal of Applied Physics*, 63(10):3711–3713, 1988.

[13] Ananth Kamath. Exploring linear and non-linear ac susceptibilities of single crystal gadolinium around curie & spin-reorientation transitions. Master's thesis, Dec 2022.

[14] Kanthal. Kanthal, a wire. `https://www.kanthal.com/en/products/material-datasheets/wire/resistance-heating-wire-and-resistance-wire/kanthal-a/`.

[15] Movaffaq Kateb, Jon Tomas Gudmundsson, and Snorri Ingvarsson. Effect of atomic ordering on the magnetic anisotropy of single crystal ni80fe20. *arXiv preprint arXiv:1903.00105*, 2019.

[16] Charles Kittel. *Introduction to Solid State Physics*. John Wiley & Sons, 8th edition, 2004.

[17] K. P. Kämper, W. Schmitt, G. Güntherodt, R. J. Gambino, and R. Ruf. Cro: A half-metallic ferromagnet. *Physical Review Letters*, 59(22):2788–2791, 1987.

[18] L.D. Landau. On the theory of phase transitions. *Zhurnal Eksperimental'noi i Teoreticheskoi Fiziki*, 7:19–32, 1937.

[19] J.A. Mydosh. Spin glasses: An experimental introduction. *Taylor and Francis*, 1993.

[20] Sunil Nair and A. Banerjee. Probing a ferromagnetic critical regime using nonlinear susceptibility. *Physical Review B*, 68:094408, 2003.

[21] D.S. Negi, R.P. Pant, and P.A. Alvi. Design and development of an ac magnetic susceptibility setup for high temperature measurements. *Measurement*, 44(10):1878–1883, 2011.

[22] G. Shirane, K. Ishida, and H. Takagi. Nonlinear susceptibility of ni near the curie temperature. *Journal of the Physical Society of Japan*, 64(3):951–954, 1995.

[23] Stanford Magnets. Magnetic moments: The basic information. 2024.

[24] Y. Tian et al. Magnetic domain structure in nanocrystalline nickel electrodeposits. *Journal of Applied Physics*, 123(23):234301, 2018.

[25] Michael Tinkham. *Introduction to Superconductivity*. Dover Publications, Mineola, NY, 2nd edition, 2004.

[26] Shashwat Tomar. Probing ultra-slow magnetisation relaxation in transition metal fluorides through dc and ac magnetometry. Master's thesis, May 2023.

[27] C. V. Topping and S. J. Blundell. A.c. susceptibility as a probe of low-frequency magnetic dynamics. *Journal of Physics: Condensed Matter*, 31(1):013001, 2019.

[28] Wikipedia contributors. Critical exponent, 2023.

[29] J.M. Yeomans. *Statistical Mechanics of Phase Transitions*. Oxford University Press, 1992.

[30] Kai-Xuan Zhang, Hanshu Xu, Jihoon Keum, Xiangqi Wang, Meizhuang Liu, and Zuxin Chen. Unexpected versatile electrical transport behaviors of ferromagnetic nickel films. *arXiv preprint arXiv:2402.14275*, 2024.